Pontifícia Universidade Católica
do Rio de Janeiro

Mengen Liu

Plastic Stress Concentration Effects in Fatigue Strength

Dissertação de Mestrado

Dissertation presented to the Programa de Pós-graduação em Engenharia Mecânica of PUC-Rio in partial fulfillment of the requirements for the degree of Mestre em Engenharia Mecânica.

Advisor:	Prof. Marco Antonio Meggiolaro
Co-advisor:	Prof. Jaime Tupiassú Pinho de Castro

Rio de Janeiro
March 2023

Pontifícia Universidade Católica
do Rio de Janeiro

Mengen Liu

Plastic Stress Concentration Effects in Fatigue Strength

Dissertation presented to the Programa de Pós-graduação em Engenharia Mecânica of PUC-Rio in partial fulfillment of the requirements for the degree of Mestre em Engenharia Mecânica. Approved by the Examination Committee:

Prof. Marco Antonio Meggiolaro
Advisor
Departamento de Engenharia Mecânica – PUC-Rio

Prof. Jaime Tupiassú Pinho de Castro
Co-advisor
Departamento de Engenharia Mecânica – PUC-Rio

Prof. Antonio Carlos de Oliveira Miranda
Departamento de Engenharia Civil e Ambiental – UnB

Prof. Renato Bichara Vieira
Departamento de Engenharia Mecânica – PUC-Rio

Rio de Janeiro, March 27th, 2023

Mengen Liu

The author graduated in Mechanical Engineering from Pontifícia Universidade Católica do Rio de Janeiro in 2021.

Bibliographic data

Liu, Mengen

Plastic stress concentration effects in fatigue strength / Mengen Liu ; advisor: Marco Antonio Meggiolaro ; co-advisor: Jaime Tupiassú Pinho de Castro. – 2023.
63 f. : il. color. ; 30 cm

Dissertação (mestrado)–Pontifícia Universidade Católica do Rio de Janeiro, Departamento de Engenharia Mecânica, 2023.
Inclui bibliografia

1. Engenharia Mecânica – Teses. 2. Concentração de tensão à fadiga. 3. Tolerância a trinca curta não propagante. 4. Gradiente de tensão. 5. Plasticidade localizada no entalhe. 6. Curva S-N. I. Castro, Jaime Tupiassú Pinho de. II. Miranda, Antonio Carlos de Oliveira. III. Pontifícia Universidade Católica do Rio de Janeiro. Departamento de Engenharia Mecânica. IV. Título.

CDD: 621

Acknowledgments

First of all, I want to thank God for His countless blessings, graces and joys.

My sincere gratitude to my parents and sisters, for their unconditional support and love.

To my advisor Prof. Jaime T. P. de Castro for sharing his knowledge and encouraging words. To my co-advisor Prof. Antonio C. O. Miranda for his contributions, patience and guidance throughout my studies. To Prof. Marco A. Meggiolaro for his help.

To CNPq and PUC-Rio, for the aid granted, without which this work could not have been accomplished. This study was financed in part by the Coordenação de Aperfeiçoamento de Pessoal de Nível Superior – Brasil (CAPES) – Finance Code 001; and by the Fundação de Amparo à Pesquisa do Estado do Rio de Janeiro (FAPERJ) – Processo SEI-260003/014622/2022.

Abstract

Liu, Mengen; Meggiolaro, Marco Antonio (Advisor). **Plastic stress concentration effects in fatigue strength**. Rio de Janeiro, 2023. 63p. Dissertação de Mestrado – Departamento de Engenharia Mecânica, Pontifícia Universidade Católica do Rio de Janeiro.

Elasto-plastic stress gradient factors ahead of notch tips are used to evaluate actual notch effects in fatigue strength, quantified by fatigue stress concentration factor K_f. Usually, it is smaller than the linear elastic stress concentration factor of the notch, K_t, due to material tolerance to non-propagating short cracks. Considering that local plasticity around notch tips plays a significant role in the growth behavior of short cracks within the notch plastic zone, a sound mechanical methodology is proposed to account for the effects of elasto-plastic stress and strain fields in the actual K_f value. Two-dimensional finite element analyses are conducted to compute stress intensity factors of smooth and notched specimens. Ramberg-Osgood model and Neuber's rule are used to achieve approximations for strain-based intensity factors. For methodology validation, numerical predictions are compared to experimental stress-life data of center, U, and V-notched plate specimens made of different materials and tested under uniaxial load ratios of -1, 0, and 0.1 collected from the literature. The comparisons show good agreement proving that the elasto-plastic solution provides more accuracy than the linear elastic one. The most discrepant results are obtained at load ratios of 0 and 0.1, and they can be significantly improved if non-zero mean stress effects are considered.

Keywords

Fatigue stress concentration; tolerance to non-propagating short crack; stress gradient; notch plasticity; S-N curve.

Resumo

Liu, Mengen; ; Meggiolaro, Marco Antonio (Advisor). **Efeitos plásticos de concentração de tensão na resistência à fadiga**. Rio de Janeiro, 2023. 63p. Dissertação de Mestrado – Departamento de Engenharia Mecânica, Pontifícia Universidade Católica do Rio de Janeiro.

Neste trabalho, o fator de gradiente de tensões elastoplástico na frente da raiz de entalhe é utilizado para investigar o efeito real do entalhe na resistência à fadiga, quantificado pelo fator de concentração de tensões à fadiga, K_f. Este é geralmente menor que o fator de concentração de tensões do entalhe, o parâmetro linear elástico K_t, devido à tolerância do material a trincas curtas não propagantes. Considerando que a plasticidade localizada na vizinhança da raiz do entalhe afeta o comportamento de crescimento de trincas curtas dentro da zona plástica induzida pelo entalhe, uma abordagem baseada na Mecânica da Fratura é proposta para abranger os efeitos dos campos de tensões e deformações elastoplásticas no cálculo do K_f. Análises bidimensionais por elementos finitos são adotadas para calcular fatores de intensidade de tensão de espécimes planos e entalhados. O modelo de encruamento de Ramberg-Osgood e a regra de Neuber são usados para obter aproximações de fatores de intensidade baseados em deformação. Para validação da metodologia, as previsões numéricas geradas são comparadas com dados experimentais de S-N coletadas da literatura para espécimes com K_t. Estes possuem furo circular central ou entalhes tipo U ou V, são feitos de diferentes materiais e testados sob cargas axiais com razão igual a -1, 0 ou 0,1. A comparação mostra boa concordância e prova que a solução elastoplástica proporcione maior precisão do que a linear elástica. Os resultados mais discrepantes são obtidos em razões de carga de 0 e 0,1, no entanto, eles podem ser significativamente melhorados quando é considerada a correção de efeitos de tensão média não nula.

Palavras-chave

Concentração de tensão à fadiga; tolerância a trinca curta não propagante; gradiente de tensão; plasticidade localizada no entalhe; curva S-N.

Table of contents

List of figures

List of tables

List of symbols and abbreviations

a	Crack size
a_0, a_R	Short crack characteristic size under stress ratio R=0 or any generic R
a_{max}	Maximum tolerable non-propagating short crack
E	Young's modulus
ε, ε_n	Strain, nominal strain
H, h	Strain-hardening constant and exponent
H_c, h_c	Cyclic strain-hardening constant and exponent
K_t	Stress concentration factor
K_f	Fatigue stress concentration factor
$K_{f,EP}$	Elasto-plastic fatigue stress concentration factor
K_I	Stress intensity factor (mode I)
$\Delta K_{th,0}$, $\Delta K_{th,R}$	Fatigue crack propagation threshold under stress ratio R=0 or any generic R
K_{gr}	Stress gradient factor
γ	Adjustable data-fitting parameter
R	Stress ratio
S_L	Fatigue limit
σ, σ_n	Stress, nominal stress
q	Notch sensitivity factor

EP	Elasto-plastic
FCG	Fatigue crack growth
FCI	Fatigue crack initiation
LE	Linear elastic
SBIF	Strain-based intensity factor
SCF	Stress concentration factor
SGF	Stress gradient factor
SIF	Stress intensity factor

1
Introduction

Most structural components have notches, the genetic name of geometric details associated with abrupt geometric changes like holes, slots, grooves, keyways, shoulder, corners, threads, weld fillets, etc, which are necessary for their assembly and/or operation. Notches locally increase stresses and strains around their tips and are preferred sites for fatigue crack initiation (FCI) and initial growth under cyclic service loads during operational tasks. Notch effects on fatigue strength must be investigated in structural integrity assessments to guarantee that notched components can work safely during their entire designed functional lives.

Stress concentration factors (SCF), K_t are defined by the ratio of the maximum stress in the notch tip to the nominal stress, $K_t = \sigma_{max}/\sigma_n$. It is a linear elastic (LE) parameter dependent on the notch geometry and on the load type. However, the actual notch effects on fatigue strength are quantified by the fatigue SCF, K_f, which is defined by the ratio of the fatigue limit of a un-notched and polished specimen to that of a corresponding notched specimen, $K_f = S_L/S_{L,notch}$. Generally, K_f is smaller than K_t and its value depends not only on the K_t, but also on notch tolerance to short cracks. Such tolerance is known to be a function of its K_t, of the stress gradient ahead of the notch tip, and of two primary material resistances to fatigue, namely, the fatigue limit $S_L(R)$ and the fatigue crack growth (FCG) threshold $\Delta K_{th}(R)$ at a given stress ratio, $R = \sigma_{min}/\sigma_{max}$.

Fatigue damage is associated with two driving forces. The FCI stage is controlled by the stress or strain range and by the stress peak at the critical point, i.e., $\Delta\sigma$ (or $\Delta\varepsilon$) and σ_{max}; and the FCG stage by the range and the peak of the stress intensity factor (SIF), i.e., ΔK and K_{max}. In this way, both fatigue stages appropriately consider the stress amplitude and the mean (or peak) stress effects. For this reason, the material FCI limit and its long crack FCG threshold, $S_L(R)$ and $\Delta K_{th}(R)$ are written as functions of stress ratio R to indicate this two-driving forces dependence.

In complex engineering components, crack-like defects are commonly detected at critical notch roots, the preferred site for FCI. Some fatigue cracks keep growing under cyclic operational loads and should be repaired before they reach a critical size and provoke catastrophic failures. Others, however, stop after growing for a little and then become non-propagating when a nominal stress $S_L(R)/K_t < \sigma_n < S_L(R)/K_f$ is applied. The use of short crack tolerance concepts is indispensable for modeling this behavior.

Cracks are called *short* as long as their FCG threshold is dependent also on the crack size a, thus $\Delta K_{th}(a, R) \leq \Delta K_{th}(R)$. They usually are also physically small and typically have lengths smaller than 1mm [1]. Short cracks may be classified as microstructurally short or mechanically short cracks. The former have sizes up to the grain size, i.e., $a \leq gr$; the latter are larger but still small enough so that ΔK_{th} remains dependent on crack lengths. Microstructurally short cracks grow within a non-isotropic region affected by microstructural details like grain boundaries and second phase particles. Their FCG behavior is of interest for material science, but they are too small to be mapped in field applications, which limits their usefulness for practical mechanical design and preventive maintenance purposes. Hence, in this work, short cracks refer to mechanically short ones only.

While FCG rates of long cracks can be well modeled using the Linear Elastic Fracture Mechanics (LEFM) parameter SIF, it is well known that FCG rates of short cracks behave differently before converging into those of the long cracks [2-5]. A newly initiated crack has a tip embedded into a local plastic zone, either induced by a notch or by the own crack tip, which typically has an extent comparable to the short crack size. This condition makes the traditional LEFM parameter SIF insficient to quantify the inelastic stress fields near crack tips.

Also, experimental works on the stress-life behavior of notched components show that their K_fs tend to reduce at short lives and high fatigue loads, as illustrated by the graph from an early NACA technical note shown in Figure 1.1 [6]. Notice that the K_f vs. K_t trend has a nonlinear behavior for all stress levels, with a larger variation for sharper notches, and that $K_f \rightarrow 1$

when the entire notched body plastifies and other failure mechanisms become predominant.

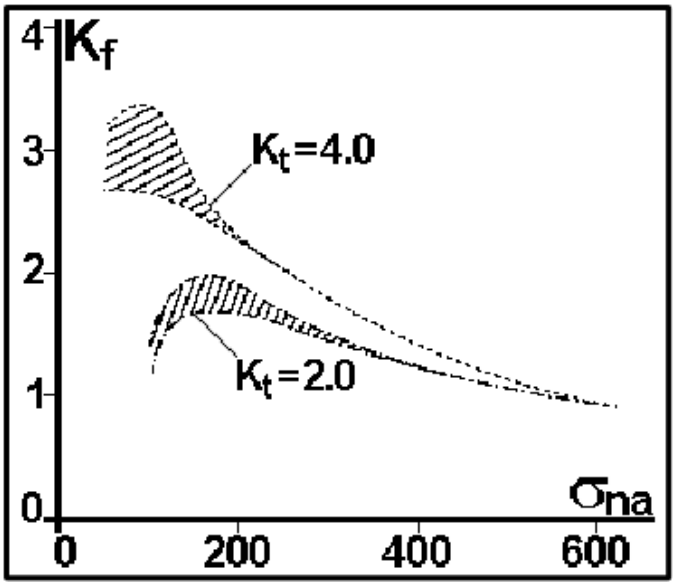

Figure 1.1. The effect of Kt and the maximum nominal stress on Kf [6].

Classic stress-life (S-N) procedures for modeling FCI are still widely used to analyze and design structural components that work under nominally linear elastic (LE) conditions and supposedly free of crack-like defects in practical engineering applications. Thus, S-N procedures are applicable only when the critical point peak stresses of defect-free components are smaller than the cyclic yield strength of the material. Thus, albeit fatigue damage is caused by gradual accumulation of cyclic EP strains, S-N procedures do not explicitly quantify any plastic effects that act at such critical points neither recognize the presence of cracks. That is why the S-N method is only suitable for predicting long FCI lives. Despite its severe limitation, the S-N method is highly useful in practice, because most fatigue problems in real-life applications are associated with nominally LE stresses at critical points, since most structural components are designed for long service lives.

Given the importance of the S-N method in fatigue designs and some limitations in its concepts, this work aims to study the effects of locally yielded stress concentrators on S-N curves. For this, modeling of tolerance to small defects with small-scale plasticity is proposed to be incorporated into the conventional S-N method.

1.1 Summary

The dissertation is organized as follows:

Chapter 1 introduces the background of and motivations for this work. As we discussed a lot about non-propagating short cracks, the reasons why they are of concern will also be justified throughout the next chapters and especially in Section 3.4.

Chapter 2 provides a concise literature review of previous research on similar or related fields.

Chapter 3 presents several basic concepts to establish a theoretical framework for the present study.

Chapter 4 shows a numerical method to solve LE K_f problems and, in addition, it proposes a methodology developed with some suitable modifications to include elasto-plastic behavior based on consolidated concepts.

Then, Chapter 5 describes the validation procedures using data collected from the literature. Additionally, the results obtained are shown.

Finally, a conclusion and some considerations for future works are presented in Chapter 6.

All citations are listed in the References.

2
Literature review

Kirsch [7], Inglis [8], Neuber [9], Savin [10], Peterson [11], and Heywood [12] are all well-known pioneers in LE K_t studies and applications. Based on a few data points, Peterson [13] proposed semi-empirical expressions for the notch sensitivity factor q of steels and aluminum alloys, where the notch sensitivity factor $0 \leq q \leq 1$ is used to relate K_t to its corresponding $K_f = 1 + q \cdot (K_t - 1)$. His expressions still are widely used for mechanical design purposes (although they are not applicable to model elongated notches [14]). Frost*, et al.* [15] introduced significant contributions in the late 1950s when they discovered that FCI from notch tips could generate non-propagating cracks.

Figure 2.1 shows that non-propagating cracks are generated under $S'_L/K_t < \sigma_{na} < S'_L/K_f$, where σ_{na} is the applied nominal stress amplitude and S'_L is fatigue limit of the material. Figure 2.2 detected a small crack initiated early in the specimen life at a 1.3mm deep V-notch with a very sharp radius tip $\rho \cong 70\mu m$, which did not propagate after $2.4 \cdot 10^7$ load cycles in a low-C steel rotary bending specimen tested under a relatively low nominal stress range $\Delta\sigma = 78MPa$. These data indicate that K_f values can be associated with small non-propagating fatigue cracks emanated from notch tips. The physical reasons for this seemingly odd behavior will be discussed later.

The importance of tolerance to short cracks in FCG modeling is not a novelty. FCG modeling taking into account the particular behavior of short cracks has been studied by other researchers.

Non-propagating short cracks can also be found in smooth specimens. Abdel-Raouf*, et al.* [17], [18] claim that cracks can emanate from a free surface due to inherent microstructurally dependent strain concentration phenomena. The lack of constraint at the surface may result in the highly strained grains that form a preferred site for crack initiation. In the interior of the material, the constraint increases, and strain concentration decays at a rate that is inversely proportional to the grain size.

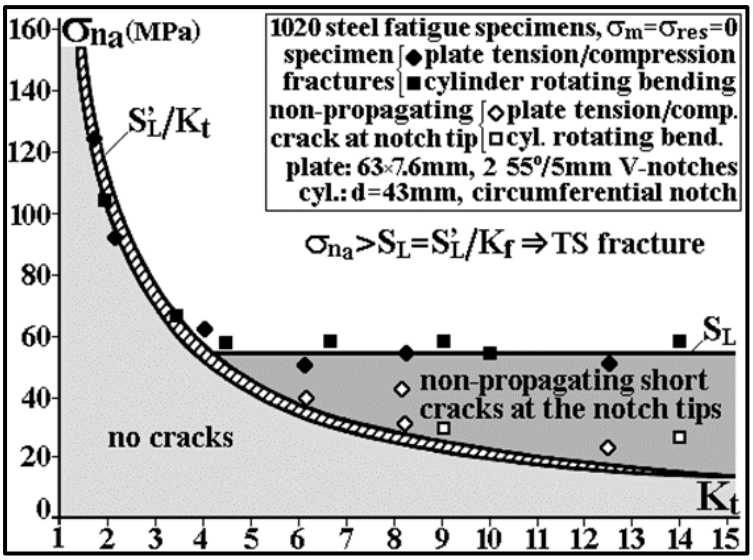

Figure 2.1. Experimental data of test specimen fractures and non-propagating cracks in 1020 steel under R=0 [16].

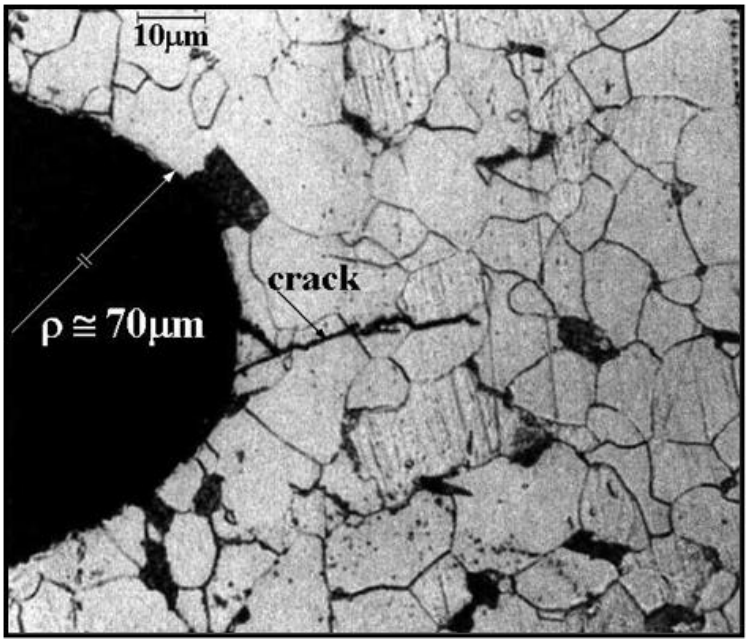

Figure 2.2. A small crack initiated at a sharp notch tip and did not propagate after 2.4×10^7 cycles [15].

Therefore, once the maximum driving force of the crack at the surface decreases and reaches a value below the threshold for fatigue crack growth, it becomes non-propagating.

Chapetti [19] proposed a local extension force concept related to the strain concentration phenomena, which affects the microstructurally short crack regime and only the beginning of the mechanical small crack regime. Thus, surface non-propagating cracks are generally microstructurally short, and their modeling depends on the specimen's microstructural details, such

as anisotropy. As discussed earlier, the present work aims to analyze the behavior of mechanically (not microstructurally) short cracks using solid mechanics methodologies applicable to size scales larger than the grain size.

Sadananda*, et al.* [20], [21, 22] developed methods to model propagating or non-propagating conditions of incipient cracks initiated at stress concentrations under EP stress fields for various notch K_t values and root radii, using Unified Approach concepts. In addition to the FCG driving forces, ΔK and K_{max}, the Unified Approach claims that the corresponding FCG thresholds, ΔK_{th} and $K_{max,th}$ should be both surpassed as well for fatigue cracks to propagate.

Noroozi*, et al.* [23] introduced the unified two-driving force UniGrow model to account for residual stress effects induced by reversed cyclic plasticity at the crack tip and quantified by the residual SIF $K_{I,r}$ on FCG.

Modifications of the UniGrow model have been proposed to incorporate short and long-crack FCG characteristics [3, 24, 25]. Bang and Ince [3] proposed a novel FCG model that assumes the UniGrow thresholds ΔK_{th} and $K_{max,th}$ are crack-length dependent and capable of accurately predicting crack growth in both short and long-crack regimes.

The non-propagating short-crack approach is mechanically sounder than other approaches based on stress averages computed ahead of the notch tip. Antunes*, et al.* [26] have suggested that the use of Stress Gradient Factors (SGF) to modify appropriately the SIFs of short cracks that depart from notch tips indicates that any critical distance is related to these SIFs and not to material size parameters, like the grain size for instance. Notch sensitivity should be renamed stress gradient sensitivity to consider similar behaviors in fretting, residual stress fields in welds, and other critical point types associated with significant stress gradients.

As discussed earlier, the LEFM-based FCG driving forces, ΔK and K_{max} are unable to describe the short crack regime when local plasticity must be considered in FCG analyses. Surveys on how local plasticity affects FCG also have been conducted by various researchers.

To incorporate the plasticity-induced stress redistribution around the crack tip in FCG modeling, Ince and Glinka [27] developed a new model to

determine the elasto-plastic (EP) stress-strain analysis near a crack tip using approximations based on LE stress fields.

El Haddad, Smith and Topper [5] showed that a strain-based intensity factor (SBIF) and a short crack characteristic length together are capable of accounting for small-scale yielding near notch tips, by replacing the stress term with a strain term, as well as providing a good description of the short crack FCG regime. This idea is fundamental for the development of the present work.

Dowling [28] proposed the J-integral range ΔJ as the FCG driving force for short cracks emanating from notches to account for plasticity corrections. In addition, El Haddad*, et al.* [29] modified Dowling's J-integral by including the characteristic short crack length to reduce the discrepancy between the FCG behavior of short and long cracks.

Furthermore, from the operational viewpoint, it is indispensable to understand whether and how a notch can affect the component at different levels depending on the operating load level.

Majzoobi and Daemi [30] investigated the effects of notch geometry on fatigue lives for low-strength (LS) and high-strength (HS) steels. For LS steels, they observed that fatigue stress concentration factors K_f depend on the fatigue life, and they vary from a low value for low-cycle fatigue tests to a higher value for high-cycle fatigue tests. On the other hand, no significant variation of the K_f value was observed in HS steels.

The ASM Handbook [31] claims that K_f reduces at high stress levels for steels, and that such variations occur due to a reduction of the notch effect by plastic deformation.

Juvinall and Marshek [32] say that some authors even recommend neglecting the effect of notches at short fatigue lives around 10^3 cycles, but they claim this practice is valid only for relatively LS metals. For relatively HS alloys, they say that notch effects at short and long lives (around 10^6 cycles) are nearly equal. Thus, they recommended the use of the high-cycle LE K_f in all cases, including the medium and low-cycle FCI regimes. This practice is straightforward, but may be overly conservative in low-cycle fatigue, where significant cyclic yielding occurs around the notch tip.

This short review indicates that the K_f variation with stress level for finite FCI lives is well known and properly supported by experimental data in the literature. However, for situations in which macroscopic plastic strains exist around notch tips and cannot be neglected in K_f modeling, there is still a lack of reliable models to predict notch sensitivity for medium and low-cycle FCI regimes.

Miranda*, et al.* [33] proposed a method based on SGF and short crack concepts to predict K_fs for high-cycle FCI regime, under nominally LE conditions around the notch tip. This idea is extended in the present dissertation to EP conditions. We can treat the inelastic behavior of the material at the notch root using Neuber's rule of stress and strain concentrations [34] and the strain-hardening Ramberg-Osgood relation. This way, we can predict K_fs based on EP solutions and they should be called elasto-plastic $K_{f,EP}$ in order to be distinguished from the traditional LE K_f.

Hence, this work aims to model the effects of local plasticity on material tolerance to small defects, and to comprehend how they may affect conventional S-N curves that are extensively used in fatigue designs of general engineering components for long lifetimes.

3
Theoretical fundamentals

Usually, the major part of the operational fatigue lives of real structural components is spent initiating and propagating short cracks, which have a much larger importance on long fatigue life predictions than long cracks do. The LEFM SIF ΔK_I quantify the cyclic driving force of long fatigue cracks by

$$\Delta K_I = \Delta\sigma\sqrt{\pi a} \tag{3.1}$$

where $\Delta\sigma$ is the nominal stress range, and a is the crack length.

For the crack to grow by fatigue, the loadings {ΔK, K_{max}} or the equivalent {ΔK, R} shoud be larger the corresponding R-dependent FCG threshold, i.e., $\{\Delta K, R\} \geq \Delta K_{th}(R) = \Delta K_{th,R}$. However, short cracks with size $a \to 0$ propagate under SIF ranges smaller than $\Delta K_{th,R}$. Indeed, if they had to obey $\{\Delta K, R\}(a \to 0) \geq \Delta K_{th,R}$, then the nominal stress range would need to be $\Delta\sigma = \Delta K_{th,R}/\sqrt{\pi a} \to \infty$. In reality, no material would support that.

Although traditional LEFM concepts do not apply to model short cracks, a sequence of sound LEFM techniques can be used instead if their peculiarities are correctly considered:

i. a predominantly LE stress field surrounds them;
ii. the material is isotropic and homogeneous in its size scale;
iii. their crack-size dependent FCG threshold is smaller than the long-crack size independent threshold, $\Delta K_{th,R}(a) < \Delta K_{th,R}$.

This chapter discusses procedures used to model the FCG behavior of LE mechanically short cracks that depart from notch tips. Short crack concepts, stress gradient ahead of notch tips, and the physical reasons for short crack stops or arrests are reviewed here as well.

3.1
Short cracks behavior

To deal with the seemingly odd behavior of short cracks, El Haddad,

et al. [35], [36, 37] proposed a practical solution modifying the original formulation for ΔK_I, eq.(3.1) by introducing a hypothetical short crack characteristic length, a_0, where the subscript refers to the stress ration, R=0 in this case. The resulting El Haddad-Topper-Smith (ETS) model is given by:

$$\Delta K_I = \Delta\sigma\sqrt{\pi(a+a_0)}, \text{ where } a_0 = (1/\pi)\cdot\left(\Delta K_{th,0}/\Delta S_{L,0}\right)^2 \qquad (3.2)$$

where $\Delta K_{th,0} = \Delta K_{th}(R=0)$ is the FCG threshold for long cracks and $\Delta S_{L,0} = 2S_L(R=0)$ is the fatigue limit of the material, both under pulsating loads $R=0$. Now, the modified ΔK_I can describe the FCG of any cracks, short or long.

According to eq.(3.2), there are two FCG thresholds: long fatigue cracks ($a \gg a_0$) grow when $\Delta K_I = \Delta\sigma\sqrt{\pi a} > \Delta K_{th,0}$; and short cracks ($a \to 0$) grow when $\Delta\sigma > \Delta S_{L,0}$. Such hypotheses reproduce very well the tendency of experimental data of needed stress range for FCG as a function of the crack length, i.e., $\Delta\sigma \times a$, in Kitagawa-Takahashi diagrams, delineating the transition between fatigue crack propagation and non-propagation regimes**,** see Figure 3.1. Two boundary lines of threshold stress range are shown: one for short cracks that is equal to fatigue limit, $\Delta\sigma_0 = \Delta S_{L,0}$; and another for long cracks determined in function of FCG threshold, $\Delta\sigma = \Delta K_{th,0}/\sqrt{\pi a}$. They together limit the region of non-propagating cracks zone at $R=0$, which is also well delineated by the ETS curve, when,

$$\Delta\sigma \le \Delta K_{th,0}/\sqrt{\pi(a+a_0)} \qquad (3.3)$$

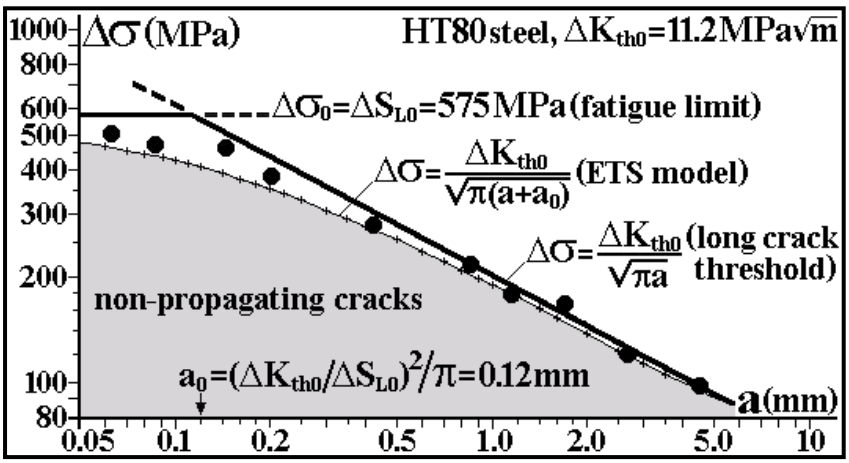

Figure 3.1. A typical Kitagawa-Takahashi diagram of stress range needed to grow fatigue

cracks of any size at R=0 [38].

In addition, the SIF of cracked components usually includes a geometry factor $g(a/w)$, and Yu*, et al.* [39] used it to generalize eq.(3.2):

$$\Delta K_I = \Delta\sigma\sqrt{\pi(a+a_0)}\cdot g(a/w), \quad \text{where } a_0 = (1/\pi)\cdot\left\{\Delta K_{th,0}/\left[\Delta S_{L,0}\cdot g(a/w)\right]\right\}^2 \tag{3.4}$$

It is worth noting that since most cracks initiate at notch tips, their FCI driving force is the local maximum stress range $\Delta\sigma_{max} = K_t \cdot \Delta\sigma_n$. On the other hand, most SIF equations use the nominal $\Delta\sigma$, and all geometrical effects are corrected by $g(a/w)$. Besides, the stress gradients ahead of notch roots play a significant role in the tolerance to short cracks on FCG analyses. The concepts of stress gradients will be discussed ahead.

For now, it is helpful to divide the geometry correction factor $g(a/w)$ into three multiplicative factors:

$$g(a/w) = \eta \cdot K_{gr}(a/w)\cdot f(a/w) \tag{3.5}$$

where a constant $\eta = 1.1215$ quantifies free surface effects; the stress gradient factor (SGF) $K_{gr}(a/w)$ quantifies stress gradients ahead of notch tips ($K_{gr}(a\to 0)\to K_t$) at notch tips; and the geometry factor $f(a/w)$ quantifies all other geometry effects far from the notch tip, e.g., those caused by specimen boundaries. Thus, eq. (3.4) can be rewritten:

$$\Delta K_I = \eta \cdot K_{gr}(a/w)\cdot \Delta\sigma\sqrt{\pi(a+a_0)}\cdot f(a/w), \quad \text{where } a_0 = (1/\pi)\cdot\left[\Delta K_{th,0}/\left(\eta\cdot\Delta S_{L,0}\right)\right]^2 \tag{3.6}$$

Note that a_0 only considers the free surface effect. To prevent FCI, stress ranges at notch tips must be smaller than the material fatigue limit, $\Delta\sigma(a\to 0) = K_t\Delta\sigma_n = K_{gr}(a\to 0)\Delta\sigma_n < \Delta S_{L,0}$. Thus, stress gradient effects quantified by $K_{gr}(a/w)$ are not needed in thei case. Moreover, for short cracks $f(a\to 0)\to 1$.

However, from the operational viewpoint, SIFs are FCG driving forces, thus should not be material-dependent. A convenient solution is to use the short crack characteristic size a_0 to modify FCG thresholds instead of SIFs.

This way, the material property FCG threshold turns into a function of crack size and fatigue limit:

$$\frac{\Delta K_{th,0}(a)}{\Delta K_{th,0}} = \frac{\eta \cdot K_{gr}(a/w) \cdot \Delta\sigma\sqrt{\pi a} \cdot f(a/w)}{\eta \cdot K_{gr}(a/w) \cdot \Delta\sigma\sqrt{\pi(a+a_0)} \cdot f(a/w)} = \sqrt{\frac{a}{a+a_0}} \tag{3.7}$$

Thus, the crack size-dependent FCG threshold, $\Delta K_{th,0}(a)$ is given by an expression that depends on the long-crack FCG threshold, fatigue limit, and crack size:

$$\Delta K_{th,0}(a) = \Delta K_{th,0}[1 + (a_0/a)]^{-\frac{1}{2}} \tag{3.8}$$

Bažant [40] proposed an adjustable data-fitting parameter γ to fit the long crack and short crack limit behaviors of a wide range of materials:

$$\Delta K_{th,0}(a) = \Delta K_{th,0}\left[1 + (a_0/a)^{\frac{\gamma}{2}}\right]^{-\frac{1}{\gamma}} \tag{3.9}$$

For γ = 2, eq.(3.9) yields the original ETS model from eq.(3.8); and for $\gamma \to \infty$, it reproduces the bilinear limits of the Kitawaga-Takahashi diagram with $\Delta\sigma = \Delta S_{L,0}$ for the short cracks ($a < a_0$) and $\Delta\sigma = \Delta K_{th,0}/\sqrt{\pi a}$ for the long ones ($a \gg a_0$) as shown in Figure 3.1.

This additional data-fitting parameter improves the modeling of data on short crack FCG thresholds, see Figure 3.2, where most data lay within the zone between $\gamma = 1.5$ and $\gamma = 8$ curves. Figure 3.3 illustrates the influence of the γ parameter on the stress thresholds required to propagate either short or long cracks under $R = 0$ in a Kitagawa-Takahashi diagram, given by:

$$\Delta\sigma_0(a) = \frac{\Delta K_{th,0}}{\sqrt{\pi a}}\left[1 + (a_0/a)^{\frac{\gamma}{2}}\right]^{-\frac{1}{\gamma}} \tag{3.10}$$

Non-propagating cracks can exist below the lines, i.e., when the applied stress is smaller than the minimum stress range needed for a short or long crack to grow, $\Delta\sigma_0(a)$. Again, the bilinear limit behavior is reproduced by $\gamma \to \infty$.

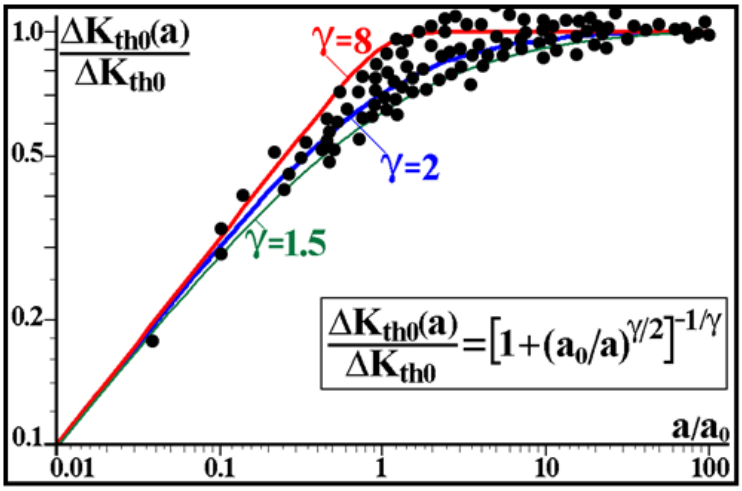

Figure 3.2. The use of various parameters *γ* allows a better data-fitting of short crack FCG thresholds experimentally measured [38].

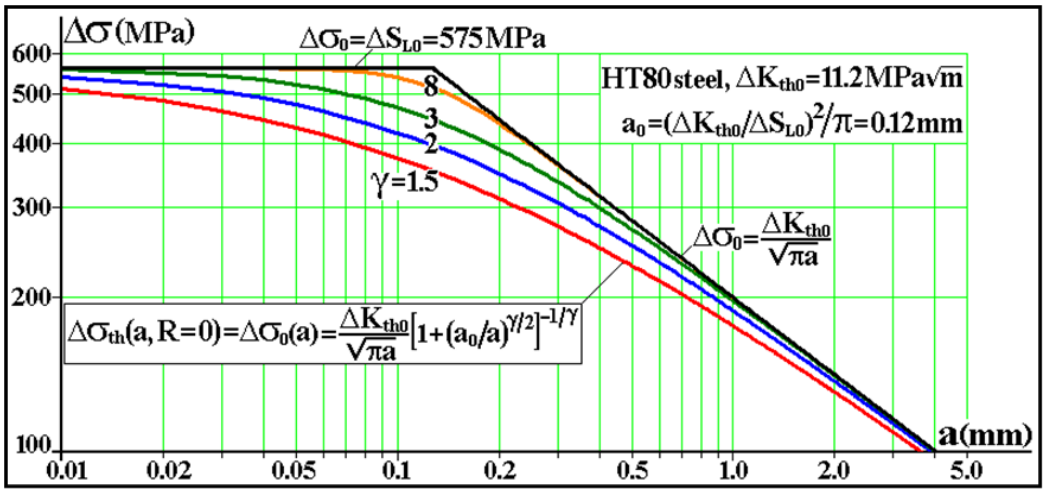

Figure 3.3. Effect of parameter *γ* on the shape of crack size dependent fatigue limit curves of a Kitagawa-Takahashi diagram [38].

Furthermore, it is indispensable to generalize the above concepts to other stress ratios *R*, since FCG has two driving forces, ΔK and K_{max}. For eq.(3.9) to consider effects of K_{max} or *R*, that is, peak or mean stress effects on FCG, it can be rewritten as:

$$\Delta K_{th,R}(a) = \Delta K_{th,R}\left[1 + (a_R/a)^{\frac{\gamma}{2}}\right]^{-\frac{1}{\gamma}}, \qquad a_R = (1/\pi)\cdot\left[\Delta K_{th,R}/\left(\eta\cdot\Delta S_{L,R}\right)\right]^2 \tag{3.11}$$

where a_R is short crack characteristic length at *R*, $\Delta K_{th,R}(a) = \Delta K_{th}(a,R)$ is the crack size dependent FCG threshold, $\Delta K_{th,R}$ is the FCG threshold of long cracks ($a \gg a_R$) and $\Delta S_{L,R} = \Delta S_L(R)$ is the material fatigue limit, all at a given stress ratio R.

3.2
Stress gradient factors

Stress gradients ahead of notch roots are significant in FCG analyses, because they are needed to explain the behavior of short cracks that initiate at notch tips and then stop propagating and become tolerable cracks.

The SGF $K_{gr}(a/w)$ in eq.(3.6) quantifies the effects of localized stress gradients on SIFs. Abrupt geometry or load transitions can cause significant SGFs, e.g., notches, fretting, contact between bodies, concentrated loads, and residual stresses caused by plasticity, welding, quenching, cold-forming, and (or) thermal stresses.

Mode I SIF ranges are given by $\Delta K_I = \Delta\sigma\sqrt{\pi a} \cdot g(a/w)$, where $g(a/w)$ quantifies the effects that affect the SIF besides the stress range $\Delta\sigma$ and the crack length a. In Figure 3.4(a), the SIF of a Griffith plate containing a center crack under mode I loading is calculated by eq.(3.1) for a crack length equal to $2a$. For cracks that depart from a free surface as in the semi-infinite plate of Figure 3.4(b), the free surface factor $\eta = 1.1215$ should be included to correctly calculate the SIF. Figure 3.4(c) shows a finite strip and a geometry factor $f(a/w)$ that accounts for specimen size (e.g., the width, w) and loading conditions. For very small cracks $a \to 0$, $f(a/w \to 0)$ tends to 1. Finally, Figure 3.4(d) shows a notched plate with a crack emanating from the notch root, where the local stress concentration is largest, and the stress gradient effect ahead of its tip is quantified by the SGF, $K_{gr}(a/w)$.

Thus, SGF $K_{gr}(a/w)$ is the ratio of the SIF range of a notched body to that of the corresponding reference body without notches:

$$\Delta K_I \underbrace{= \eta \cdot \Delta\sigma\sqrt{\pi a} \cdot f(a/w)}_{\Delta K_{I,ref}} \cdot K_{gr}(a/w) \;\rightarrow\; K_{gr}(a/w) = \frac{\Delta K_I}{\Delta K_{I,ref}} \tag{3.12}$$

Figure 3.5 illustrates how these three factors vary according to the crack size, i.e., while the crack tip moves away from the notch root. While η is constant, the geometry factor $f(a/w)$ starts with a unit value at the notch root and increases, and the SGF $K_{gr}(a/w)$ is initially equal to K_t at the

notch root and reduces to 1 at regions far from the notch-affected zone.

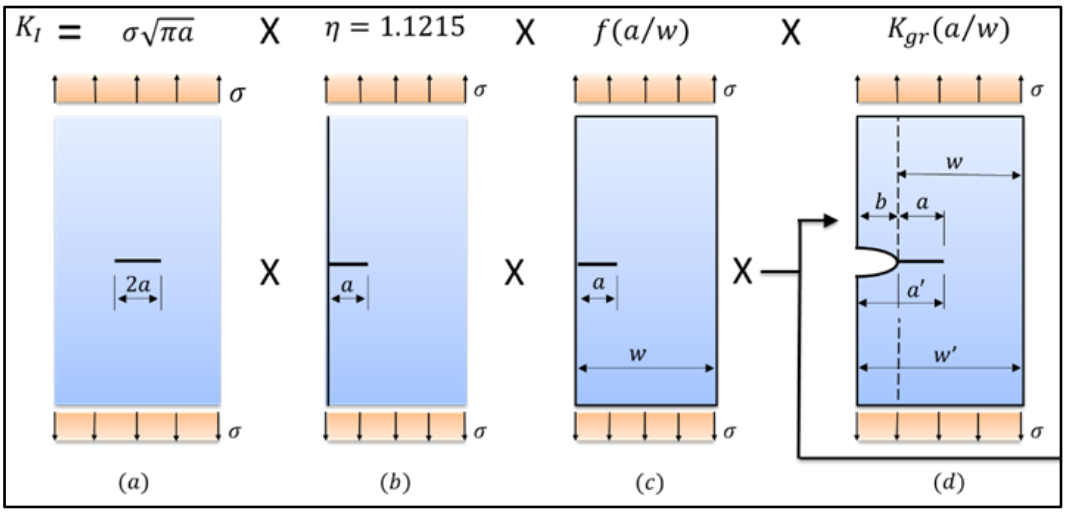

Figure 3.4. Stress gradient factor concepts [33].

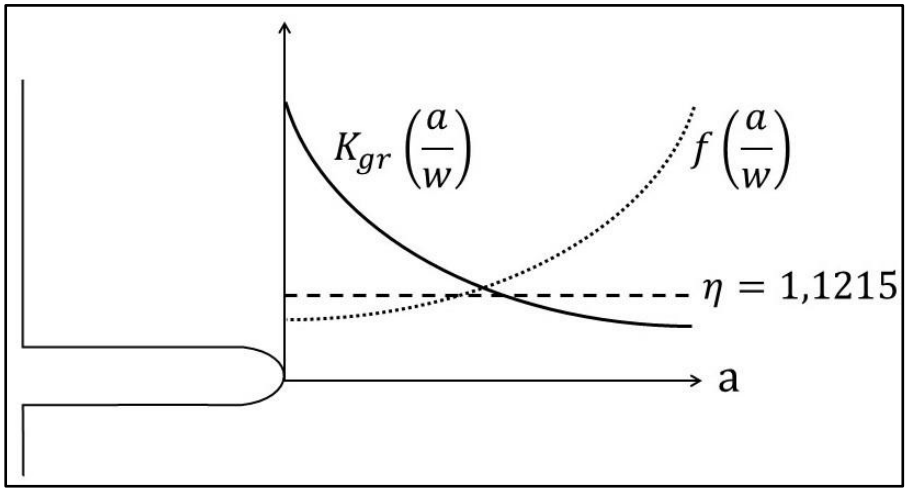

Figure 3.5. Multiplicative factors which affect the SIF: free surface correction *η*; geometry factor *f(a/w)*; and SGF K_{gr}*(a/w)*.

In general, the geometry factors $f(a/w)$ are obtained by solving the entire stress field in cracked components, through finite elements methods (FEM) or any other suitable numerical method. Since SIFs are LE parameters, the obtained solutions can be listed and used for other similar geometries. For instance, the SIF expression for the finite strip shown in Figure 3.4(c) is given, within 0.5% for any a/w, by [41]:

$$K_I = 1.1215 \cdot \sigma\sqrt{\pi a} \cdot f(a/w), \text{ where} \qquad (3.13)$$

$$f(a/w) = \left[0.671 + 1.80\frac{a}{w} + 0.329\left(1 - \sin\frac{\pi a}{2w}\right)^3\right]$$

$$\cdot \sec\frac{\pi a}{2w} \cdot \sqrt{\frac{2w}{\pi a}\tan\frac{\pi a}{2w}}$$

Analogously, when an edge notch is introduced on the finite strip, see Figure 3.4(d), the previous SIF should also include the effects of notch stress concentration and the stress gradient ahead of its tip. Thus, the final SIF of the notched plate becomes:

$$K_I = 1.1215 \cdot \sigma\sqrt{\pi a} \cdot f(a/w) \cdot K_{gr}(a/w) \qquad (3.14)$$

There are a few $f(a/w)$ solutions of simple notched components that already incorporate stress gradient effects around the notch tip. However, complete SIF solutions are rare, hence $K_{gr}(a/w)$ solutions, which can also be listed like $f(a/w)$, are useful in several cases. This work uses eq.(3.14) as the general expression for mode I SIFs, explicitly separating the various correction factors.

Stress gradients are largest at notch tips, then they decrease and reach $K_{gr}(a/w) = 1$ from a certain distance a/w from the tip onwards. The stress gradient affected zone extension depends on notch characteristics. Sharp notches have high K_ts and steep stress gradients, thus, they affect SIFs severely but only within a small region ahead of their tips. On the other hand, smooth notches have smaller K_ts and smoother stress gradients, so they affect SIFs more slightly but for a longer stretch.

Therefore, sharp notches have very high stress concentration at their tips and severe stress gradients ahead of them. The $K_{gr}(a/w)$ is high near the notch tip, where cracks are tiny, but it decays steeply to 1 as the cracks get a bit larger. Such competition between an increasing crack size a and a simultaneously decreasing local stress $\sigma(a)$ due to the stress gradient ahead of the notch tip is the mechanical cause of why non-propagating short cracks exist, as experimentally detected by Frost, Marsh and Pook [15]. Notice that the former is beneficial while the latter is unfavorable for SIFs to arise, and the driving force must be larger than the FCG threshold so cracks can propagate.

If the SIF of a crack that departs from a notch tip becomes smaller than the FCG threshold, the crack stops. This is why the fatigue SCF K_f can (and should) be modeled as a short crack propagation problem [14, 26, 33, 42-48].

3.3 Non-propagating short crack modeling

Considering the short crack size dependent FCG threshold $\Delta K_{th,R}(a)$ and its characteristic size a_R, both given by eq.(3.11) for any R-ratio, three situations can occur with FCG behavior of a short crack growing inside a stress field with a steep gradient, e.g., near a notch tip, see Figure 3.6. Notice the notation $\Delta K_{th,R}(a, a_R)$ refers to the pair $\Delta K_{th,R}(a)$ and a_R.

a) The driving force $\Delta K_I(a) > \Delta K_{th,R}(a, a_R)$ for all crack lengths, see Figure 3.6(a). In this case, a crack initiates at a notch tip and grows continually until the end of the load history or the component fractures.

b) Initially $\Delta K(a) > \Delta K_{th,R}(a, a_R)$, the short crack starts and grows, increasing its length across a decreasing stress field ahead of the notch (whose gradient is quantified by its SGF) tip. The crack growth stops when its $\Delta K(a)$ curve crosses with the crack-size dependent $\Delta K_{th,R}(a, a_R)$ FCG threshold. If the FCG threshold remains time-independent and the driving forces keep fixed, the crack becomes non-propagating, see Figure 3.6(b).

c) Similar to (b), but the SIF $\Delta K(a)$ curve is tangent to to the FCG threshold $\Delta K_{th,R}(a, a_R)$ curve at a certain crack size a instead of crossing it. This is the limiting condition to have a non-propagating crack, and the tangent point defines the maximum size a_{max} that a non-propagating short crack can reach under the given loading and material conditions, see Figure 3.6(c). According to Castro et al. [59], a maximum short crack size a_{max} limits the crack growth/stop behavior. Thus, the tangency condition between the driving force and FCG threshold of the growing short crack defines a_{max}.

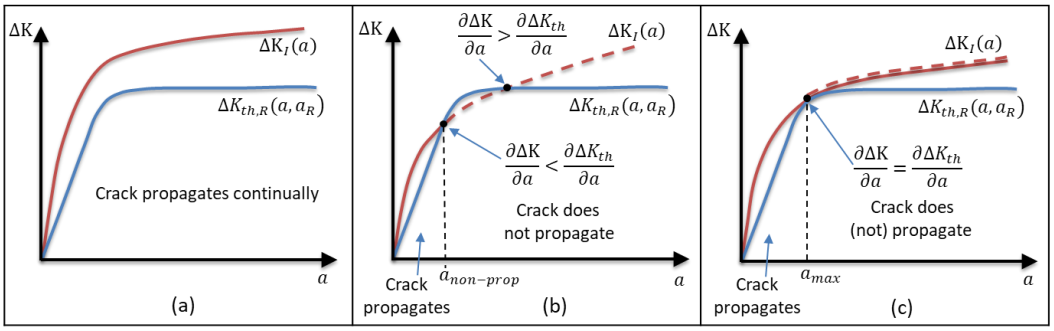

Figure 3.6. Possible FCG behaviors of short cracks initiated at sharp notch tips [49].

Since for any crack to grow, its driving force must exceed the FCG threshold:

$$\Delta K_I(a) > \Delta K_{th,R}(a) \tag{3.15}$$

The eq.(3.15) can be rewritten as below, where the right-hand side is deduced from eq.(3.11):

$$\eta \cdot K_{gr}(a/w) \cdot \Delta\sigma\sqrt{\pi a} \cdot f(a/w) > \eta \cdot \Delta S_{L,R}\sqrt{\pi a_R} \cdot \left[1 + (a_R/a)^{\frac{\gamma}{2}}\right]^{-\frac{1}{\gamma}} \tag{3.16}$$

For short cracks, $f(a/w \to 0) \to 1$, thus,

$$K_{gr}(a/w) > \underbrace{\frac{\Delta S_{L,R}}{\Delta\sigma}}_{K_f} \cdot \underbrace{\sqrt{\frac{a_R}{a}}\left[1 + \left(\frac{a_R}{a}\right)^{\frac{\gamma}{2}}\right]^{-\frac{1}{\gamma}}}_{h(a_R/a,\gamma)} \tag{3.17}$$

where $\Delta\sigma$ in this situation is the fatigue limit range of the notched body, so $\Delta S_{L,R}/\Delta\sigma = K_f$. A notation $h(a_R/a, \gamma)$ is used to simplify the representation of the equation. At the two curves tangency point, eq.(3.17) becomes an equality where $a = a_{max}$, and the derivates of both sides are also equal, so:

$$K_{gr}(a_{max}/w) = K_f \cdot h(a_R/a_{max}, \gamma) \tag{3.18}$$

$$\frac{\delta}{\delta a}\left[K_{gr}(a_{max}/w)\right] = K_f \cdot \frac{\delta}{\delta a}\left[h(a_R/a_{max}, \gamma)\right] \tag{3.19}$$

By derivating eq.(3.19), we obtain:

$$\frac{\delta}{\delta a}\left[K_{gr}\left(\frac{a_{max}}{w}\right)\right] = -K_f \cdot \frac{a_R}{2a_{max}^2\eta\sqrt{\frac{a_R}{a_{max}}}}\left[1+\left(\frac{a_R}{a_{max}}\right)^{\frac{\gamma}{2}}\right]^{-\left(\frac{1+\gamma}{\gamma}\right)} \quad (3.20)$$

The K_f term can be isolated:

$$K_f = -\frac{\delta}{\delta a}\left[K_{gr}\left(\frac{a_{max}}{w}\right)\right] \cdot \frac{2a_{max}^2\eta\sqrt{\frac{a_R}{a_{max}}}}{a_R}\left[1+\left(\frac{a_R}{a_{max}}\right)^{\frac{\gamma}{2}}\right]^{\frac{1+\gamma}{\gamma}} \quad (3.21)$$

Substituting the K_f in eq.(3.18):

$$K_{gr}\left(\frac{a_{max}}{w}\right) + 2a_{max}\eta \cdot \left[1+\left(\frac{a_R}{a_{max}}\right)^{\frac{\gamma}{2}}\right] \cdot \frac{\delta}{\delta a}\left[K_{gr}\left(\frac{a_{max}}{w}\right)\right] = 0 \quad (3.22)$$

By solving eq.(3.22), a_{max} can be found, which can be used to calculate K_f by eq.(3.18):

$$K_f = K_{gr}(a_{max}/w) \cdot \sqrt{\frac{a_{max}}{a_R}}\left[1+\left(\frac{a_R}{a_{max}}\right)^{\frac{\gamma}{2}}\right]^{\frac{1}{\gamma}} \quad (3.23)$$

This step-by-step solution provides a_{max} and K_f values in the limit condition of propagation and non-propagation of short cracks. The approach is not restricted to LE conditions since the linear elastic SGF K_{gr} can be replaced with an elasto-plastic SGF, $K_{gr\varepsilon}$, as discussed later on. A more general formulation that does not assume $f(a/w \to 0) \to 1$ for short cracks is deduced in Appendix A.

3.4
Defect tolerance in the S-N method

Classic stress-life (S-N) procedures for modeling FCI suppose defect-free components, which is impossible in practical applications since real engineering components certainly have imperfections inherent to the material manufacture or acquired during assembly or operations. Indeed, long-life fatigue designs aim to maintain service stresses at critical sites below the

fatigue limit with a suitable safety factor to avoid FCI. Still, their structural integrity cannot be assured if any of the existing small flaws, caused by any means, can grow during their service lives.

However, most mechanical components designed using the S-N approach to endure very long fatigue lives perform well in practice, indicating that they are somehow tolerant to unavoidable and practically undetectable short cracks which depart from those small defects. Although the requirement for defect tolerance quantification is self-explanatory, it is still not included in traditional FCI design routines, e.g., S-N or εN methods. In fact, these methods alone cannot quantify the defect tolerance since they do not even consider the presence of any cracks. As discussed above, this problem is solvable by adding short crack concepts to long-life design criteria. In fact, in the more straightforward constant amplitude load cases, according to eq.(3.11) and (3.15), it is enough to guarantee that:

$$\Delta\sigma < \frac{\Delta \mathrm{K}_{th,R}}{\phi_F \cdot \sqrt{\pi a} \cdot g(a/w) \cdot \left[1 + \left(\frac{a_R}{a}\right)^{\frac{\gamma}{2}}\right]^{\frac{1}{\gamma}}} \tag{3.24}$$

where, ϕ_F is a safety factor against FCI of cracks that can grow continuously due to fatigue, unlike the non-propagating short cracks we discussed above.

Thus, to guarantee structural integrity in fatigue analyses, it is necessary to evaluate the possibility of generating propagating or non-propagating cracks at critical points of the equipment, usually notch tips. This concept of non-propagating cracks leads to the idea of defect tolerance in S-N fatigue analyses for very long or infinite-life designs.

3.5
Mean stress effects

FCI depends on two driving forces, $\Delta\sigma$ or $\Delta\varepsilon$ and σ_{max}. This double dependence can also be represented by other associated parameters, e.g., in the S-N method, the alternated stress $\sigma_a = (\sigma_{max} - \sigma_{min})/2 = \Delta\sigma/2$, and the mean stress $\sigma_m = (\sigma_{max} + \sigma_{min})/2$ are commonly used instead. Usually, fatigue curves are obtained from standard tests conducted under fully reversed cyclic loading ($R = -1$ and $\sigma_m = 0$). However, when non-zero mean

stresses are applied, fatigue analyses must consider their effects. In general, tensile mean stresses, i.e., $\sigma_m > 0$, are deleterious, since they enhance crack opening and reduce fatigue lifetime, while compressive mean stresses $\sigma_m < 0$ are beneficial. Although FCI assumes there is no crack yet, in fact it is hard to define reliably the crack initiation stage due to microstructural cracks. One common practice is to define FCI stage including all fatigue process until the crack has become large enough to describe its growth by fracture mechanics. This justifies and emphasizes why tensile mean stresses are so bad for FCI.

Figure 3.7 shows some typical $\sigma_a\sigma_m$ curves. The allowable σ_a is maximum when there is no mean stress; on the other hand, when $\sigma_a = 0$, the maximum allowable mean stress is equal to a mechanical property, e.g., ultimate strength S_U at Goodman and Gerber critetion and yielding strength at Soderberg criteria. Any combinations of alternating and mean stresses on the curves are supposed to have the same fatigue lifetime. This way, $\sigma_a\sigma_m$ curves are complementary to S-N curves obtained at a constant R-ratio to reproduce the locus of the same fatigue damage.

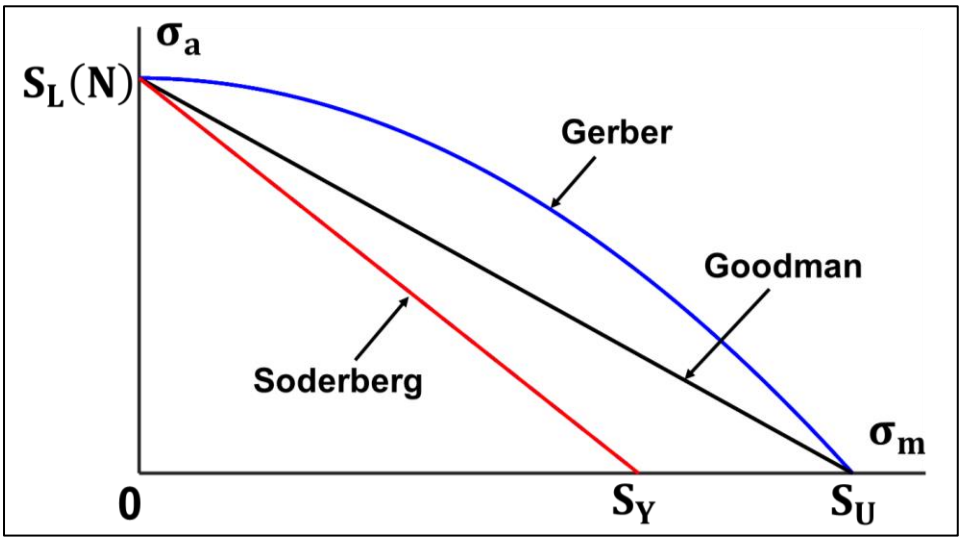

Figure 3.7. Typical alternating and mean stress curves.

Mathematically, these relations are expressed by:

Goodman: $$\frac{\sigma_a}{S_L(N)} + \frac{\sigma_m}{S_U} = 1$$

Gerber: $$\frac{\sigma_a}{S_L(N)} + \left(\frac{\sigma_m}{S_U}\right)^2 = 1 \qquad (3.25)$$

Sodeberg: $$\frac{\sigma_a}{S_L(N)} + \frac{\sigma_m}{S_Y} = 1$$

Among these and many other non-zero mean stress corrections, the relations of Goodman and Gerber are most used. The former tends to be conservative, and the latter is better in data fitting. Soderberg's relation tends to be too conservative.

3.6
Neuber's stress and strain concentration rule

The theoretical (LE) stress concentration factor, K_t, is applicable only when the material at the notch root remains elastic. Thus, $K_t = K_\sigma = K_\varepsilon$, where $K_\sigma = \sigma/\sigma_n$ and $K_\varepsilon = \varepsilon/\varepsilon_n$ are stress and strain concentration factors, respectively. For simplicity, since fatigue damage analyses are always made at critical points, it is convenient to use σ and ε to indicate the local stress σ_{max} and strain ε_{max}. When the notch root is plastically strained, the equality above is no longer valid. As yielding occurs, for ductile materials, K_σ/K_t decreases while K_ε/K_t increases, until the whole ductility is exhausted, as shown in Figure 3.8.

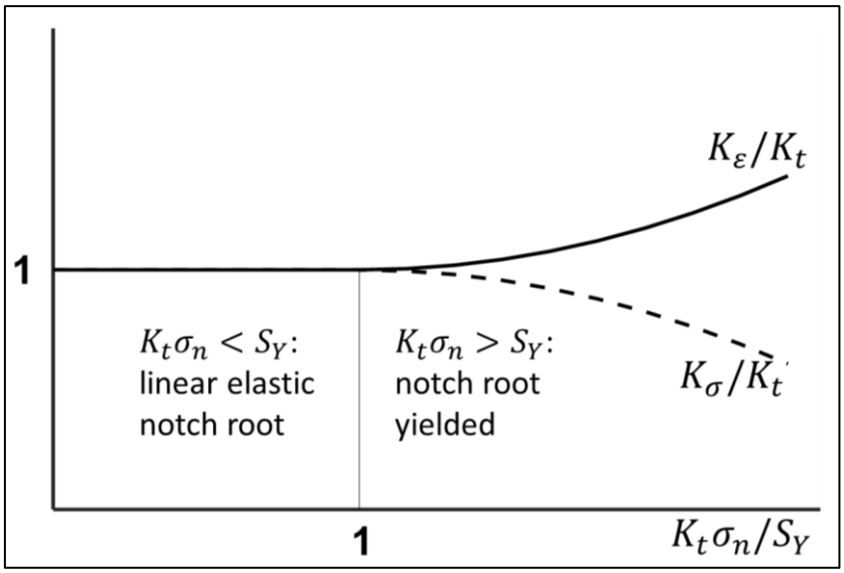

Figure 3.8. Stress and strain concentration after notch root yielded.

Neuber [34] proposed a rule which can be applied even when the material at the notch root has inelastic strains, given by:

$$K_\sigma \cdot K_\varepsilon = K_t^2 \tag{3.26}$$

Neuber's rule can be applied to cyclic loading,

$$K_t^2 = (\Delta\sigma/\Delta\sigma_n) \cdot (\Delta\varepsilon/\Delta\varepsilon_n) \tag{3.27}$$

In notch fatigue problems, some authors recommend using K_f instead of the geometrical K_t,

$$K_f^2 = (\Delta\sigma/\Delta\sigma_n) \cdot (\Delta\varepsilon/\Delta\varepsilon_n) \tag{3.28}$$

3.7 Cyclic strain hardening

To understand the material behavior of notch root when there are inelastic strains, proper modelling is necessary. Strain hardening is a gradual increase in material strength as plastic strains accumulates on most structural materials. A popular model for quantifying such behavior is the Ramberg-Osgood relation illustrated in Figure 3.9 and expressed by:

$$\varepsilon = \varepsilon_{el} + \varepsilon_{pl} = \frac{\sigma}{E} + \left(\frac{\sigma}{H}\right)^{1/h} \tag{3.29}$$

where the total strain ε is divided into an elastic part ε_{el} and a plastic part ε_{pl}, E is Young's modulus, H and h are called strain-hardening coefficient

and exponent, respectively.

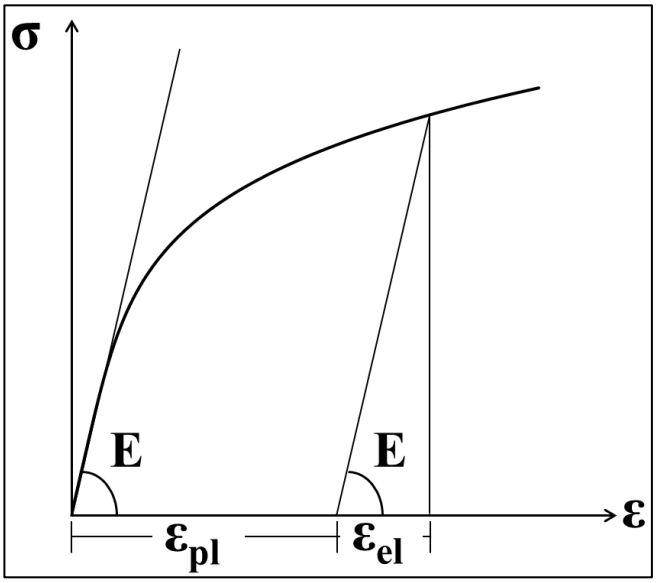

Figure 3.9. Elastic and plastic parts of a total strain $\varepsilon = \varepsilon_{el} + \varepsilon_{pl}$.

The Ramberg-Osgood model is simple and can reproduce the elasto-plastic behavior of many metallic alloys. However, it does not recognize purely elastic strains. It is worth noting the model is not a physical law, but instead, it is an adjustable equation where the parameters H and h are obtained by fitting eq.(3.29) to experimentally measured $\sigma\varepsilon$ curves.

At cyclic strain-controlled tests, the material deformation is measured as hysteresis loops, which may have a transition accompanied by either strain softening or hardening compared to the monotonic curve before reaching stabilization. The peaks of stabilized loops of tests conducted under several different strain ranges can be connected, and the obtained curve is called the cyclic $\sigma\varepsilon$ curve, as shown in Figure 3.10, which has a shape similar to the monotonic $\sigma\varepsilon$ curve described by eq.(3.29). Thus, in general, the Ramberg-Osgood model also describes well the cyclic $\sigma\varepsilon$ curves, by:

$$\varepsilon_a = \varepsilon_{el,a} + \varepsilon_{pl,a} = \frac{\sigma_a}{E} + \left(\frac{\sigma_a}{H_c}\right)^{1/h_c} \tag{3.30}$$

where, the parameters H_c and h_c are cyclic strain-hardening coefficient and exponent, and ε_a is the strain amplitude.

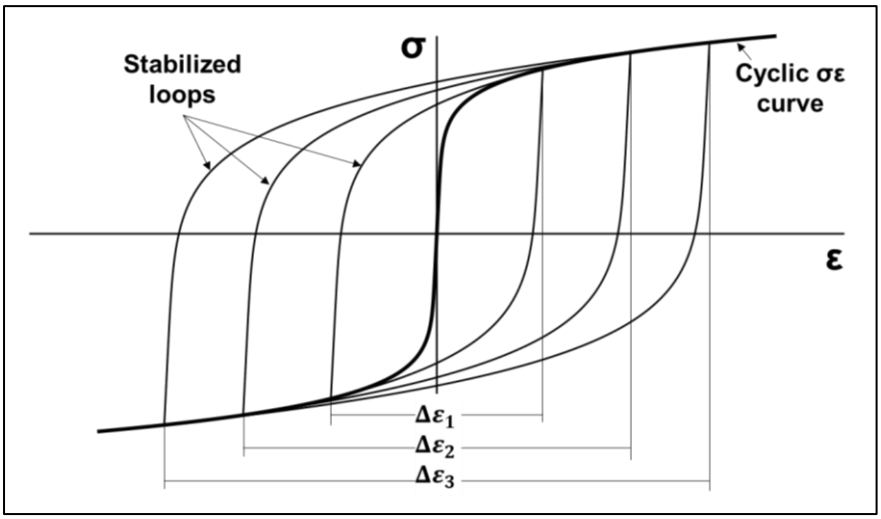

Figure 3.10. Schema of obtaining cyclic *σε* curve from peaks of several stabilized loops.

In addition, the cyclic parameters H_c and h_c can also model stabilized hysteresis loops $\Delta\sigma\Delta\varepsilon$ using the same Ramberg-Osgood cyclic parameters:

$$\Delta\varepsilon = \frac{\Delta\sigma}{E} + 2\left(\frac{\Delta\sigma}{2H_c}\right)^{1/h_c} \tag{3.31}$$

The difference between the cyclic $\sigma\varepsilon$ curve and a $\Delta\sigma\Delta\varepsilon$ loop is illustrated in Figure 3.11, where the curves are generated from the same parameters E, H_c and h_c.

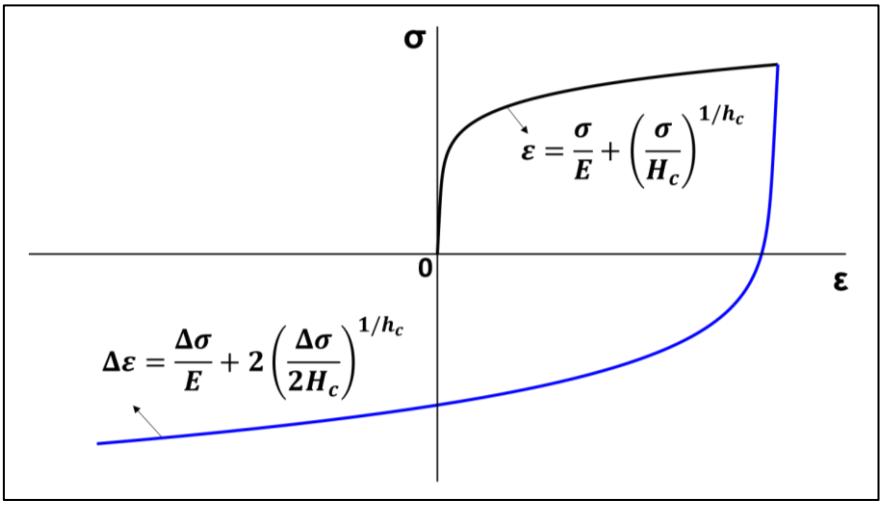

Figure 3.11. Cyclic *σε* curve and loop curve *ΔσΔε* of the same material.

4
Methodology

It is possible to obtain K_f values using analytical or even empirical approaches. However, most practical solutions employ some computational methods. In this chapter, we show a numerical way to compute K_f based on the concepts reviewed in Chapter 3. Then, the previously shown LE K_f model will be extended to include the effects of small-scale yielding around the notch tips, considering some pertinent modifications and EP fundamentals in the modeling.

4.1
Finite element solutions

SIFs can be numerically computed using weight functions. They sum up all the forces applied upon the crack faces, see an example in Figure 4.1. For this specimen, the SIF is given by:

$$K_I = \left[\frac{2P}{\sqrt{2\pi(a-d)}}\right] \cdot \left[1 + M_1\left(1-\frac{d}{a}\right)^{\frac{1}{2}} + M_2\left(1-\frac{d}{a}\right) + M_3\left(1-\frac{d}{a}\right)^{\frac{3}{2}}\right] \tag{4.1}$$

where P is a concentrated load applied perpendicularly to the crack face, d is the distance between the load and the free surface, and the M_i coefficients are specific for each crack configuration. Solutions for M_i values can be found in the literature [50-52]. Many weight functions for SIF can already be found in the literature, however, those used in this work are confidential and have not been published yet.

A notched component working under an axial force F and a moment M, as shown in Figure 4.1(b), presents a more general loading distribution. To compute the SIF of a crack of size a departing from a notch tip, the stress

distribution ahead of the notch tip can be discretized into a set of forces P_i applied on different positions d_i along the crack faces, whose $K_{I,i}$ calculated according to eq.(4.1) can be all summed up.

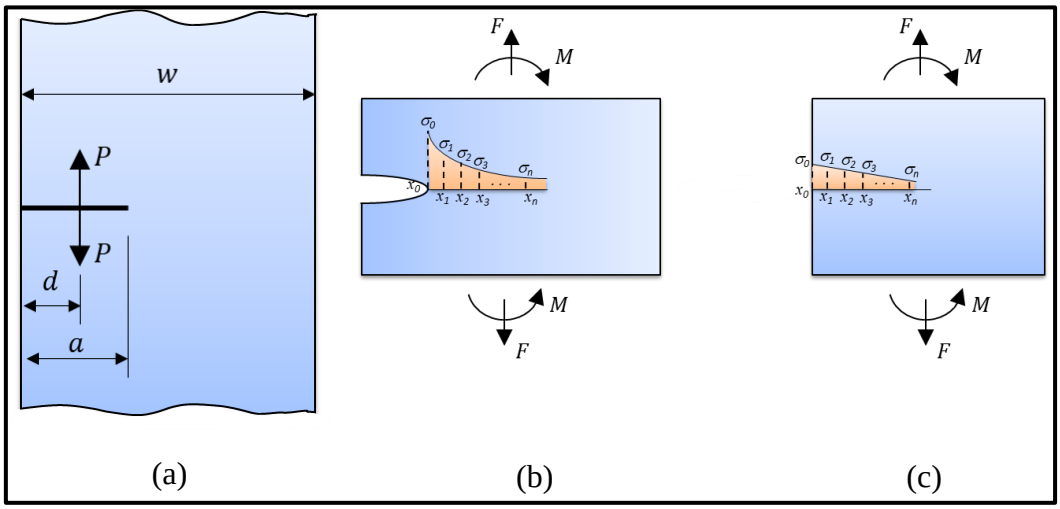

Figure 4.1. Notched and reference finite strip under axial force and moment [33].

A corresponding reference geometry considering the same axial force P and moment M is shown in Figure 4.1(c) and should be used to compute reference SIFs. The associated SGF ahead of the notch tip can be obtained based on the stress distributions of notched and reference components.

As illustrated in Figure 4.1(b) and (c), continuous stress distributions $\sigma(x)$ are discretized as $\sigma_i(x_i)$ points. For both geometries, these sets of (σ_i, x_i) can be obtained by analytical or numerical means. When the crack is parallel to the x-axis, the discrete crack size a_i from the free surface x_0 (notch tip or plain surface), the mean concentrated load P_i, and the mean distance d_i between load P_i and free surface x_0, are computed as:

$$\begin{cases} a_i = x_{i+1} - x_0 \\ P_i = (\sigma_{i+1} + \sigma_i) \cdot (x_{i+1} - x_i)/2 \\ d_i = (x_{i+1} + x_i)/2 - x_0 \end{cases} \tag{4.2}$$

For each discrete crack with size a_i, its SIF is computed by summing up the contributions of all forces $P_{j \le i}$ acting along the crack faces:

$$K_I(a_i) = \sum_{j=0}^{j=i} K_I\left(P_j, d_j, a_i, t, w\right), \forall\, i = 0, \dots, n-1 \tag{4.3}$$

The SGF can be calculated analogously to eq.(3.12) for each discrete crack size a_i, thus:

$$K_{gr}(a_i) = \frac{K_{I,notched}(a_i)}{K_{I,ref}(a_i)}, \forall\, i = 0, \dots, n-1 \tag{4.4}$$

It is necessary to convert the discrete data of $K_{gr}(a_i)$ into a continuous stress gradient distribution $K_{gr}(a/w)$ according to the procedures reviewed in section 3.3. A good fitting can be obtained using the following function type:

$$K_{gr}(a/w) = A_2 + (A_1 - A_2) \cdot \exp\left[\frac{x_0 - \ln(a/w)}{d}\right] \tag{4.5}$$

where, A_1, A_2, x_0 and d are data-fitting coefficients.

4.2
Elasto-plastic modeling of plastic K_fs

El Haddad, Smith, and Topper [5] originally proposed a strain-based intensity factor (SBIF) range, $\Delta K_{I\varepsilon}$, by replacing the stress range $\Delta\sigma_n$ with $E\Delta\varepsilon_n$. For a Griffith plate containg a center crack, as shown in Figure 3.4(a), e.g., under pulsating load $R = 0$,

$$\Delta K_{I\varepsilon} = E\Delta\varepsilon_n\sqrt{\pi(a + a_0)} \tag{4.6}$$

where, $\Delta\varepsilon_n$ is nominal strain range and a_0 is the short crack characteristic length under $R = 0$, as discussed in section 3.1.

The SBIF also applies to notched bodies even when the notch roots are locally yielded, by replacing the conventional LE stress term by an EP strain term, to model short crack FCG for both LE and EP stress and strain fields:

$$\Delta K_{I\varepsilon}(a/w) = \eta \cdot K_{gr\varepsilon}(a/w) \cdot E\Delta\varepsilon_n\sqrt{\pi(a + a_0)} \cdot f(a/w) \tag{4.7}$$

where $K_{gr\varepsilon}(a/w)$ is the plastic strain SGF.

Based on the Neuber rule given by eq.(3.27), we apply the same idea to SGFs,

$$\begin{aligned}\left[K_{gr}(a/w)\right]^2 &= \frac{\Delta K_{I\sigma} \cdot \Delta K_{I\varepsilon}}{\Delta K_{I\sigma,ref} \cdot \Delta K_{I\varepsilon,ref}} \\ &= \frac{\Delta\sigma\sqrt{\pi(a + a_0)} \cdot f(a/w) \cdot E\Delta\varepsilon\sqrt{\pi(a + a_0)} \cdot f(a/w)}{\Delta\sigma_n\sqrt{\pi(a + a_0)} \cdot f_{ref}(a/w) \cdot E\Delta\varepsilon_n\sqrt{\pi(a + a_0)} \cdot f_{ref}(a/w)}\end{aligned} \tag{4.8}$$

Considering that short cracks $f(a/w) \to 1$ and $f_{ref}(a/w) \to 1$, the equation above is simplified to:

$$\left[K_{gr}(a/w)\right]^2 = \frac{\Delta\sigma \cdot \Delta\varepsilon}{\Delta\sigma_n \cdot \Delta\varepsilon_n} \tag{4.9}$$

where $\Delta\sigma = \Delta\sigma(a/w)$ and $\Delta\varepsilon = \Delta\varepsilon(a/w)$ are the local stress and strain ranges around the crack tip, induced by the nominal stress range $\Delta\sigma_n$. Combining eq.(4.9) with the Ramberg-Osgood model for $\Delta\sigma\Delta\varepsilon$ EP loops that describes strain hardening behavior under elasto-plastic conditions, we can calculate the local EP stress and strain by solving the obtained nonlinear equation as follows:

$$\begin{aligned}\left[K_{gr}(a/w)\right]^2 \cdot \left[\Delta\sigma_n^2 + \frac{2E\Delta\sigma_n^{(h_c+1)/h_c}}{(2H_c)^{1/h_c}}\right] \\ = [\Delta\sigma(a/w)]^2 + \frac{2E[\Delta\sigma(a/w)]^{(h_c+1)/h_c}}{(2H_c)^{1/h_c}}\end{aligned} \tag{4.10}$$

Note that the cyclic Ramberg-Osgood relation is applied to the local $\Delta\sigma(a/w) \cdot \Delta\varepsilon(a/w)$ as well as to the nominal $\Delta\sigma_n\Delta\varepsilon_n$.

Finally, the EP fatigue SCF, $K_{f,EP}$, is calculated through the iterative procedures illustrated in Figure 4.2. For instance, the convergence tolerance (TOL) of iterations can be 0.01.

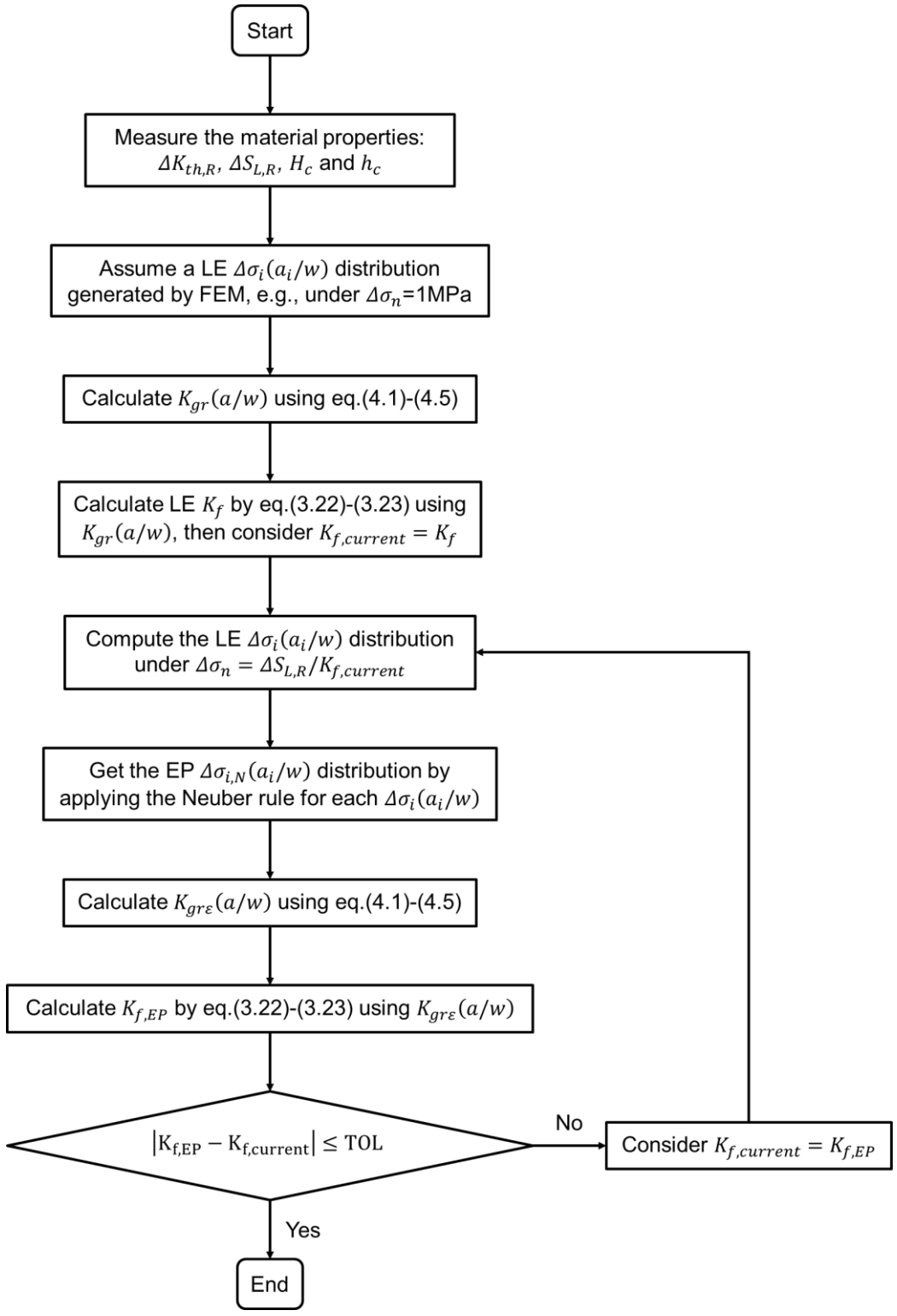

Figure 4.2. Flowchart of EP K_f.

5
Validation and results

This chapter describes the procedures used to validate the proposed methodology. The experimental stress-life (S-N) data of plain and notched specimens used in the validation were collected from [39, 53, 54].

Some limitations were established in the survey of experimental data in the literature, as detailed below:

a) The present work evaluates notch stress gradient effects under axial loadings. However, stress-life tests with this loading type are usually conducted in servo-hydraulic testing machines, which are expensive compared to S-N tests in rotary bending testing machines. This fact has made extensive axial S-N tests less viable. Consequently, few experimental data were found applicable for our validation.

b) The FCG threshold ΔK_{th} for long fatigue cracks is a fundamental property to calculate the ETS short-crack characteristic length, and so are the properties H_c and h_c, which describe the cyclic strain-hardening behavior according to Ramberg-Osgood. However, these material properties are frequently not reported by the authors of experimental works. On the other hand, estimating them may lead to quite erroneous predictions, since their values reported in the literature show very large scatter bands [55].

5.1
Comparison procedures

Initially, a straight line should be fitted to S-N data of plain specimen in a log-log plot, where a knee point N_L was set as a typical number of cycles associated with fatigue limit measurements. From the obtained line, a set of ten logarithmically evenly distributed stress range levels was determined to be the applied nominal stress ranges, $\Delta\sigma_n$ in the subsequent numerical simulations.

For each $\Delta\sigma_n$ level, LE K_f and EP $K_{f,EP}$ of the notched specimen were predicted through the proposed method, and its fatigue strength under LE

and EP conditions could be calculated by $\Delta S_{notched} = \Delta\sigma_n / K_f$ and $\Delta\sigma_n / K_{f,EP}$, respectively. Then, the predicted $\Delta S_{notched}$ values were fitted by straight lines in log-log plots too, to represent predicted S-N curves of the notched specimen using the stress gradient approach.

Finally, experimental data of S-N tests of the notched specimen were plotted on the graph and compared with the numerical prediction curves. The predictive capability of the SGF methodology can be directly verified by observing the adherence of experimental data to the EP prediction curve of notched specimens.

5.2
Material and notch geometries

Figure 5.1 illustrates the geometry of the notched specimens studied here: a) strip with a central circular hole of radius ρ; b) strip with a single U-shaped notch of depth b and radius ρ; c) strip with a single 60º V-shaped notch of depth b and radius ρ.

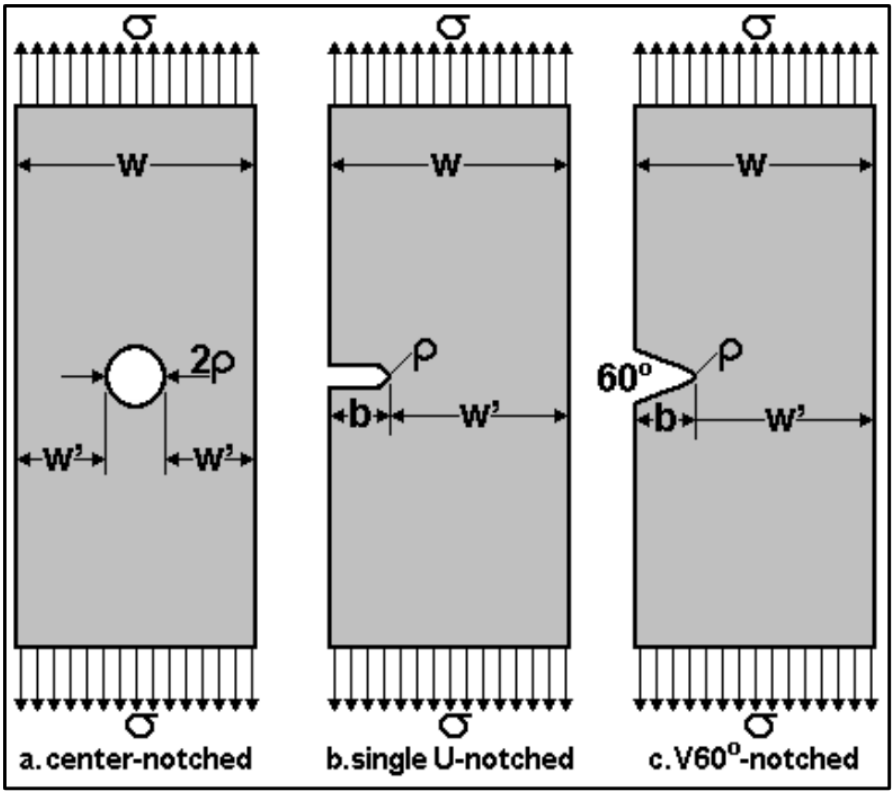

Figure 5.1. Notched specimen geometries.

All tests were conducted under axial loadings, namely, tension-compression ($R = -1$), pulsating tension ($R = 0$), or tension-tension ($R = 0.1$) loadings. The mechanical properties of the tested materials at each stress ratio are shown in Table 5.1. The ETS short-crack characteristic lengths a_R are calculated by eq.(3.11). The strain-hardening parameters of 2024-T351 and SAE1020 were directly collected from [56]. Those of SAE1045 were determined by fitting the cyclic Ramberg-Osgood expression given by eq.(3.30) to the experimental cyclic stress-strain curve using the Least squares method. It shall be noted that strain-hardening parameters may vary significantly according to the curve-fitting techniques applied to obtain them [55, 57].

Table 5.1. Materials and properties

Material	**R**	***E*** **(GPa)**	S_Y **(MPa)**	H_c **(MPa)**	h_c **(MPa)**	ΔS_L **(MPa)**	ΔK_{th} **(MPa√m)**	a_R **(mm)**
2024-T351 Al	-1	72.4	356.5	957	0.166	248	3.52	0.051
SAE1045	-1	206	390	1133	0.1696	604	9	0.056
	0	206	390	1133	0.1696	448	6.9	0.060
SAE1045 (T1200)	-1	206	645	1376	0.1661	760	7.7	0.026
SAE1045 (T900)	-1	206	1054	1417	0.1055	1134	6.98	0.010
SAE1045 (T600)	-1	206	1617	5099	0.2292	1200	7.5	0.010
SAE1020	-1	197.4	606.2	891	0.1635	412.6	16.2	0.390
	0.1	197.4	606.2	891	0.1635	327.6	11.8	0.328

Note that all SAE1045 steels have the same chemical composition but differ in the heat treatment, which modified their microstructure and hence some properties: as-received ferrite-pearlite and quenched and tempered martensite (oil quenching and tempering at 1200, 900 and 600°F, respectively, which are equivalent to 649, 482, and 315°C) [39].

Table 5.2 shows the specimen dimensions, as well as their K_t based on gross area, predicted K_f, and maximum tolerable crack length under LE conditions, $a_{max,el}$. While such conditions are considered, K_f and the associated a_{max} do not vary with applied stress level.

Table 5.2. The geometry of notched specimens

Material	R	Geometry	w (mm)	b (mm)	ρ (mm)	K_t	$K_{f,el}$	$a_{max,el}$ (mm)
2024-T351 Al	-1	Center-notched	44.6	0.12	0.12	3.02	2.175	0.053
			44.6	0.25	0.25	3.06	2.594	0.045
			44.6	0.5	0.5	3.06	2.849	0.035
			44.6	1.5	1.5	3.06	3.005	0.024
SAE1045	-1	Center-notched	44.45	0.12	0.12	3.01	2.111	0.059
			44.45	0.25	0.25	3.04	2.537	0.051
			44.45	0.5	0.5	3.05	2.815	0.040
			44.45	1.5	1.5	3.05	2.989	0.027
SAE1045	0	Center-notched	44.45	0.12	0.12	3.01	2.073	0.064
			44.45	0.25	0.25	3.04	2.502	0.055
			44.45	0.5	0.5	3.05	2.795	0.044
			44.45	1.5	1.5	3.05	2.984	0.029
SAE1045 (T1200)	-1	Center-notched	44.45	0.12	0.12	3.01	2.539	0.023
			44.45	0.5	0.5	3.05	2.962	0.014
			44.45	1.5	1.5	3.05	3.025	0.009
SAE1045 (T900)	-1	Center-notched	44.45	0.12	0.12	3.01	2.863	0.006
			44.45	0.5	0.5	3.05	3.024	0.004
			44.45	1.5	1.5	3.05	3.038	0.002
SAE1045 (T600)	-1	Center-notched	44.45	0.12	0.12	3.01	2.857	0.006
			44.45	0.5	0.5	3.05	3.023	0.004
			44.45	1.5	1.5	3.05	3.038	0.003
SAE1020	-1	Center-notched	25	4	4	3.45	3.208	0.269
			25	1.75	1.75	3.10	2.579	0.352
		U-notched	25	5	1.5	6.16	5.120	0.053
		V-notched	25	4	0.12	16.56	5.122	0.045
SAE1020	0.1	Center-notched	25	4	4	3.45	3.255	0.035
			25	1.75	1.75	3.10	2.664	0.024
		U-notched	25	5	1.5	6.16	5.289	0.059
		V-notched	25	4	0.12	16.56	5.556	0.051

5.3
Predicted S-N curves

For steels and Al alloy, the knee lives were considered at $N_L = 2 \cdot 10^6$ and $N_L = 5 \cdot 10^8$ cycles, respectively. Figure 5.2-Figure 5.5 show the predicted S-N curves for notched specimens of SAE1045 steels (in as-received and heat-treated conditions) and their experimental data under the stress ratio $R = -1$. Note that the experimental data of plain specimens are scattered because S-N tests are usually affected by various factors, e.g., the surface finish of the sample, the alignment of the testing machine and the specimens, environmental conditions, etc.

For long-life designs, when the number of cycles is larger than the knee point N_L for the material, fatigue limits of notched specimens must be obtained considering the LE K_f. Per definition, the fatigue strength against crack initiation is the stress below which the material does not accumulate fatigue damage, i.e., it must be free from macroscale cyclic plastic strains.

For each material and notched geometry, the S-N curve predicted using LE K_f is always parallel to the respective curve for plain specimens. On the other hand, numerical results show that the $K_{f,EP}$ should *diminish* with increasing stress levels, which induce larger plastic strain amplitudes around the notch tip. The different slope of the curve predicted using the EP $K_{f,EP}$ illustrates its variation according to changes in the stress level. It is intuitive since at higher stresses other failure mechanisms may become more relevant rather than FCI.

The variation in $K_{f,EP}$ is related to the stress gradient ahead of the notch tip when small-scale plastic strains are present. As the strength of the material within the plastic zone increases by strain-hardening, the maximum local stress also increases, raising the local stress gradient factors, which in turn affects the behavior of short cracks propagating there. Thus, the evaluation of cyclic Ramberg-Osgood parameters plays a fundamental role in the analysis of $K_{f,EP}$, as discussed later on.

It is worth mentioning that the fatigue life of SAE1045 steel specimens tested at $R = -1$ is plotted against the nominal elasto-plastic parameter,

$(\Delta S \Delta \varepsilon E)^{1/2} = (\Delta \sigma_n \Delta \varepsilon E)^{1/2}$, as presented by the original authors. This parameter is equivalent to the nominal stresses for notched specimens since all the applied stress levels were elastic.

Figure 5.2 shows the data obtained for specimens of as-received SAE1045 steel tested at $R = -1$, where the hole radii ρ are 0.12, 0.25, 0.5, and 1.5mm, respectively. Within this notch size range, the notch sensitivity decreases as the notch root radius decreases and the stress gradients become larger. In Figure 5.2(a), the S-N data measured in notched specimens are scattered, and most of them represent experimental K_f values between the predicted values of the LE K_f and EP $K_{f,EP}$. In Figure 5.2(b) and (c), the experimental data of notched specimens are better described by the $K_{f,EP}$ based curves, demonstrating that the fatigue notch factor indeed depends on the stress-strain conditions in the finite life region.

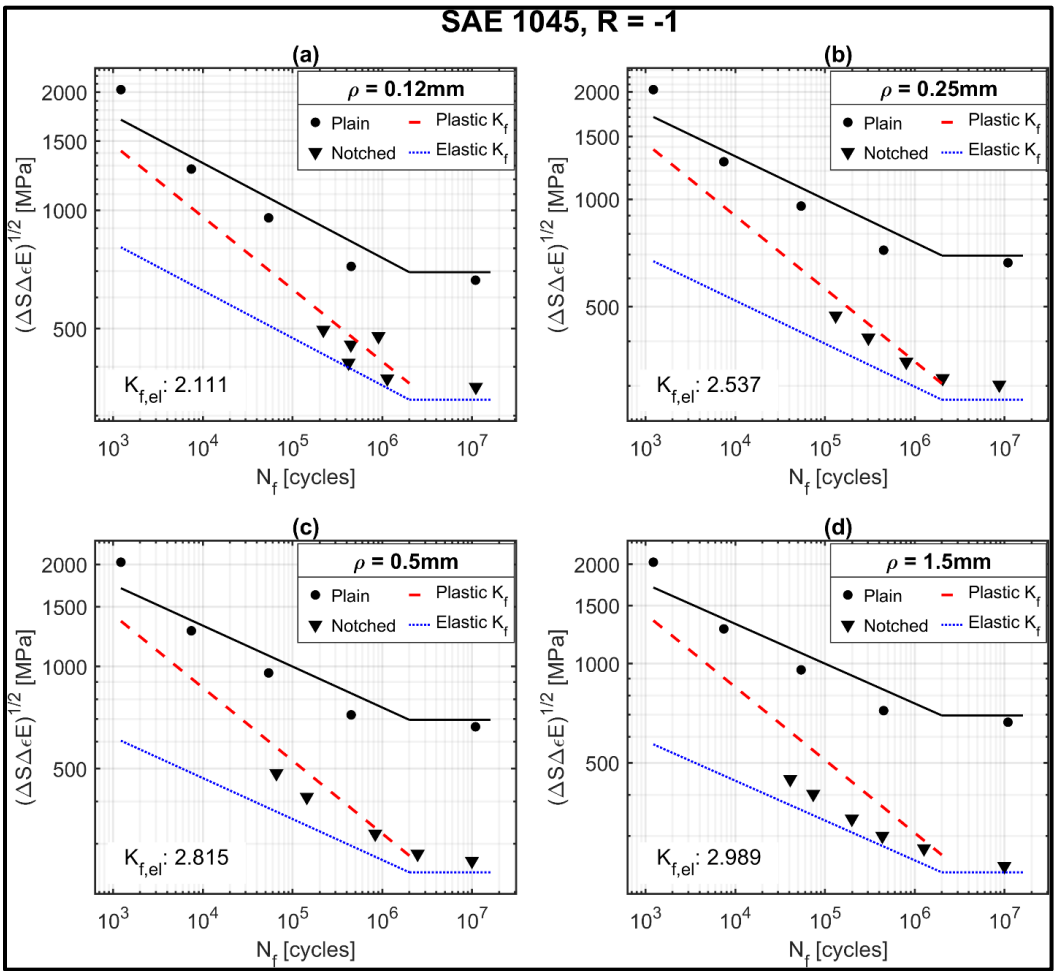

Figure 5.2. S-N curve predictions for notched SAE1045 steel specimens at R=-1.

Figure 5.3 and Figure 5.4 show data obtained for SAE1045 T1200 and T900 steels, respectively, in notched components with the radius of the central hole ρ in 0.12, 0.5, and 1.5mm. The predictions described reasonably well all experimental data: K_f values lean toward the LE prediction at lower stress levels and the EP ones at higher stress levels, where the plastic strains cannot be ignored.

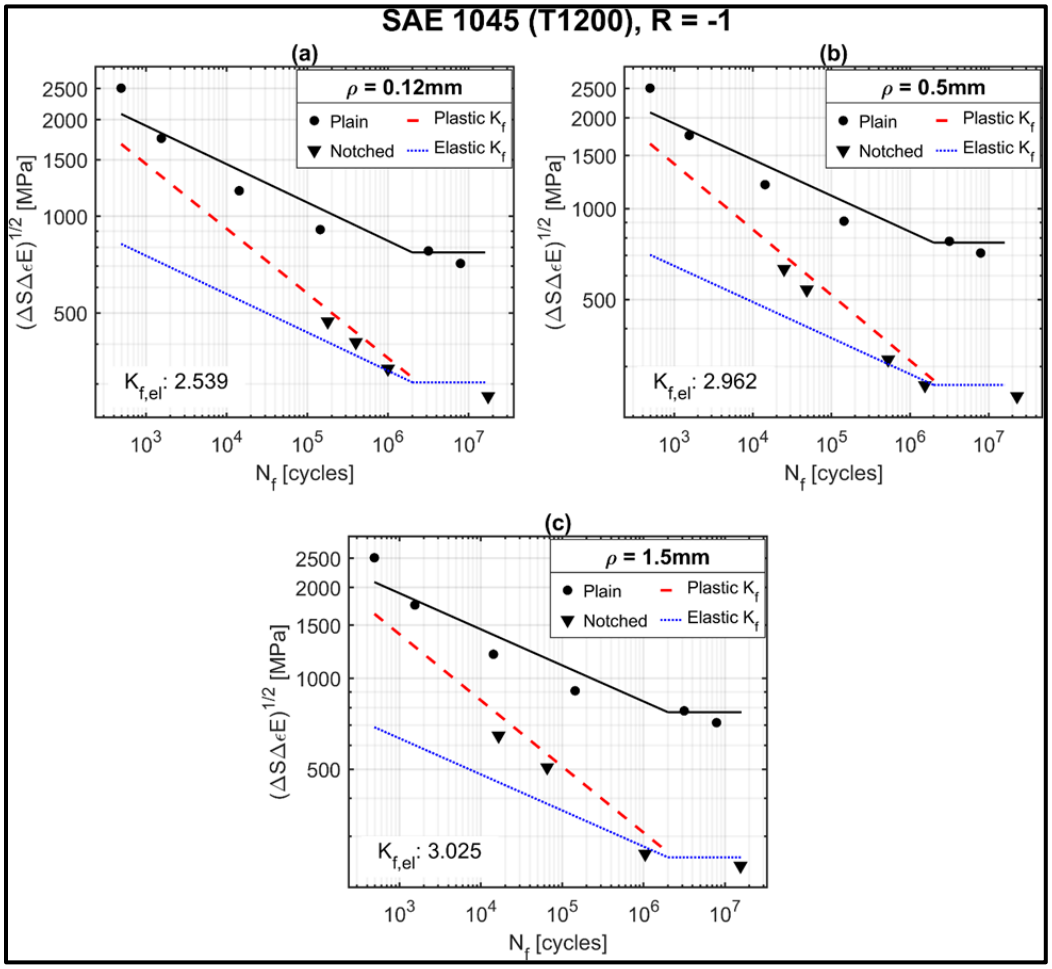

Figure 5.3. S-N curve predictions for notched SAE1045 (T1200) steel specimens at R=-1.

Figure 5.5 shows the results of SAE T600 at $R = -1$. As seen in Table 5.1, the ETS short crack lengths of SAE1045 T900 and T600 steels are very similar, despite their different fatigue limits and propagation thresholds. Consequently, the numerical model also predicted very similar LE K_f values for each geometry of these two steels. However, under EP conditions, their $K_{f,EP}$ variations in function of the stress level show different behaviors according to the cyclic strain-hardening parameters of the materials, H_c and

h_c. As the SAE1045 T600 steel substantially strengthens by plastic deformation (see their high H_c and h_c values in Table 5.1), the amplitude of local plasticity induced by elasto-plastic stresses should be smaller than it would be in the other SAE1045 steels that have lower H_c and h_c. This explains why the difference between the elastic K_f and the EP $K_{f,EP}$ predictions for T600 is smaller when compared to T900.

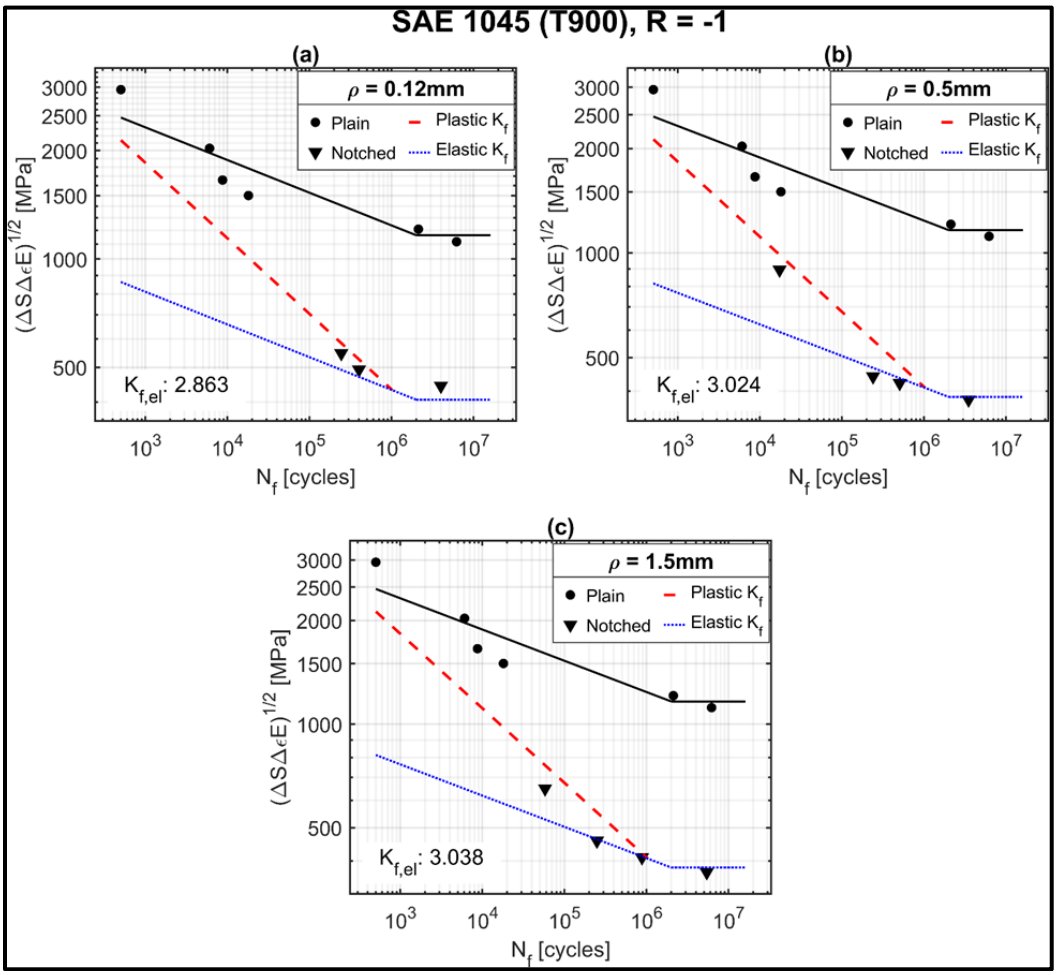

Figure 5.4. S-N curve predictions for notched SAE1045 (T900) steel specimens at R=-1.

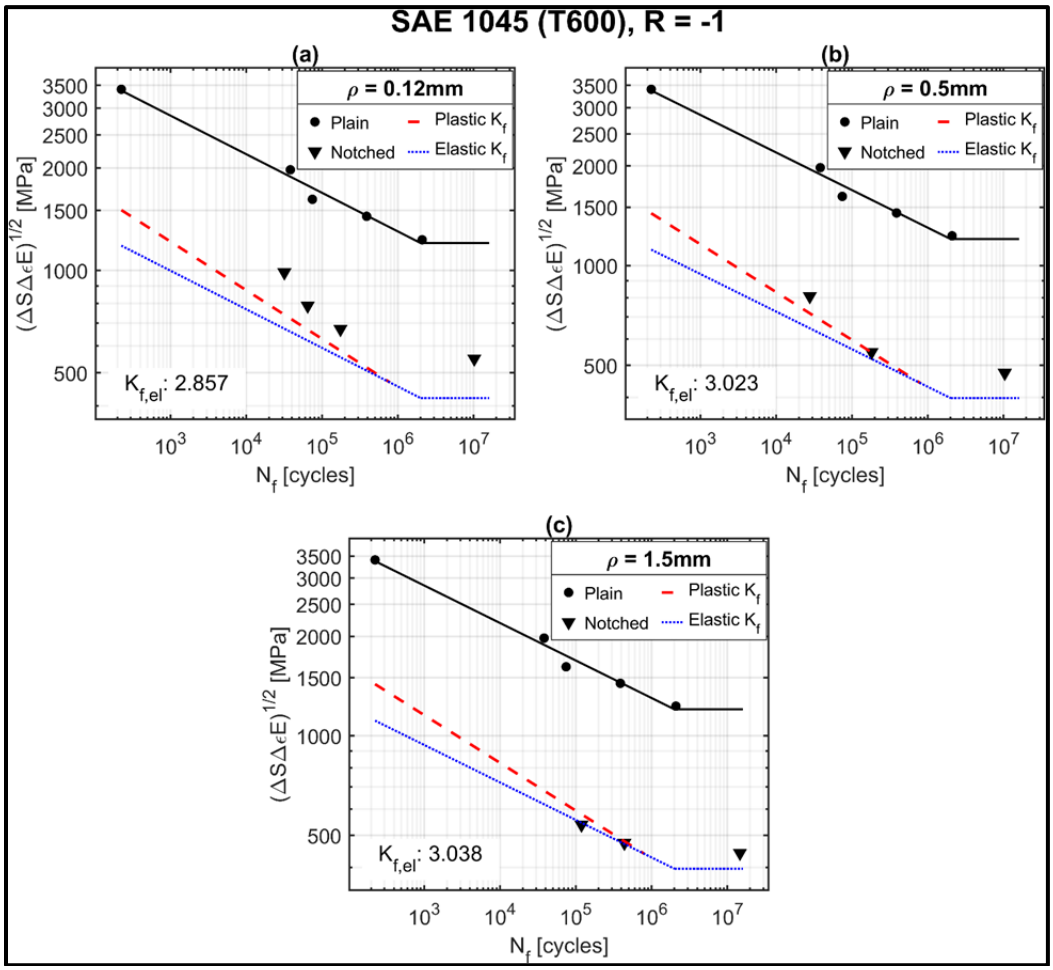

Figure 5.5. S-N curve predictions for notched SAE1045 (T600) steel specimens at R=-1.

For all analyzed notch sizes for SAE1045 T900 and T600 specimens, the predicted a_{max} lengths under LE conditions are minimal, within the range of *1*~10μm. In other words, these specimens can only tolerate very small non-propagating defects under (fixed) fatigue loads. Consequently, their LE K_fs tend to be the respective theoretical LE SCF K_t.

Nonetheless, discrepancies between the experimental data and the numerical estimates of K_fs for the SAE1045 T600 are noted in Figure 5.5. The LE K_f prediction appears to be conservative for all three notch sizes. In addition, the $K_{f,EP}$ predictions could not satisfactorily describe the experimental data in the finite-life regimes of Figure 5.5(a) and (b). The problem is possibly related to the Ramberg-Osgood parameters adjusted and used to model its strain-hardening behavior. Proper assessment of the strain field around the crack tip within the notch-induced plastic zone is essential to quantify its effect through strain-based intensity factors and to estimate EP $K_{f,EP}$.

Figure 5.6 shows predictions for notched specimens of 2024 T351 Al alloy with central hole radii ρ equal to 0.12, 0.25, 0.5, and 1.5mm. Some S-N tests on plain specimens were terminated before the fatigue life of $5 \cdot 10^8$ cycles was reached. Thus, the fatigue limit of this material was not adequately determined, which directly affects the calculation of ETS length and the subsequent K_f prediction.

Figure 5.7 shows the data obtained for the SAE1020 steel at $R = -1$. The predictions of K_f for this material at this stress ratio are conservative for all four notch geometries. On the other hand, it can be observed that the experimental K_f varies with the stress level, and the slope of the predicted elasto-plastic $K_{f,EP}$ curve can describe this trend well, although conservatively in general.

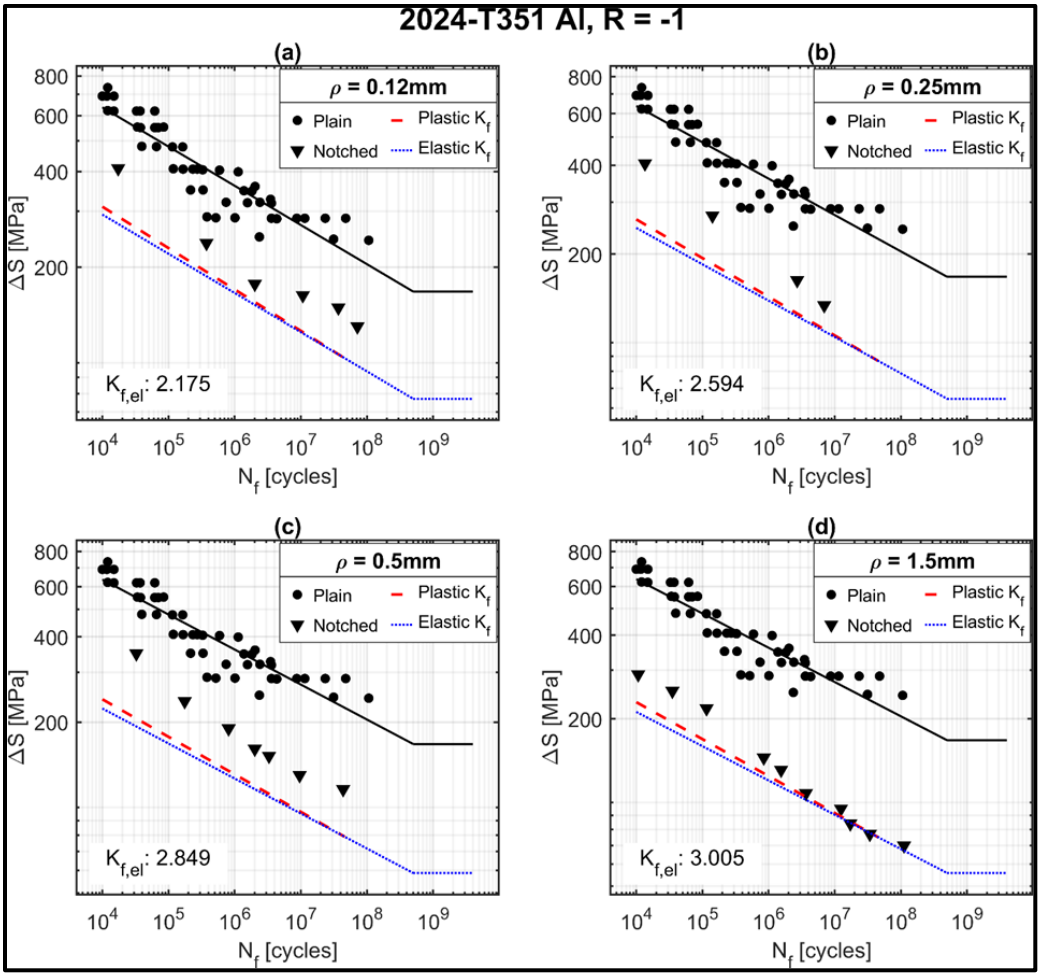

Figure 5.6. S-N curve predictions for notched 2024 T351 Al alloy specimens at R=-1.

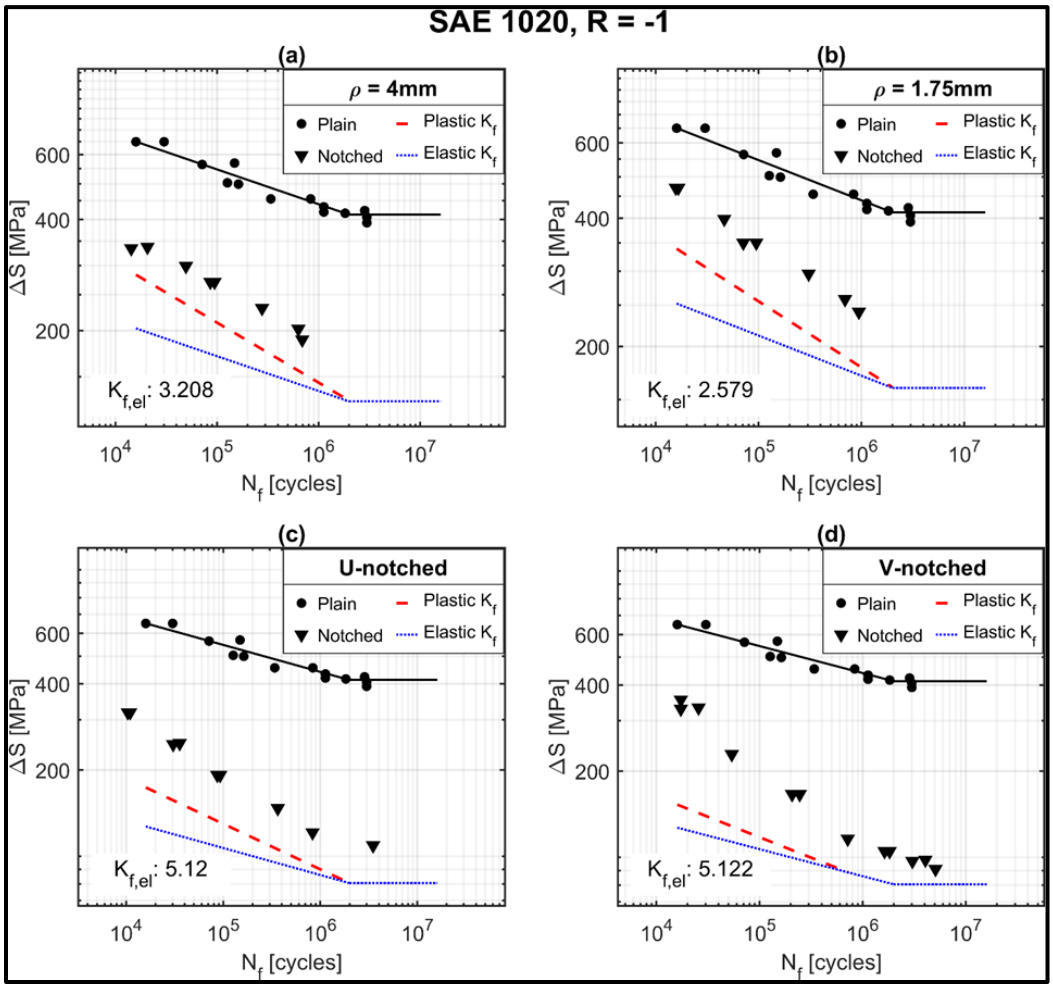

Figure 5.7. S-N curve predictions for notched SAE1020 steel specimens at R=-1.

5.4
Non-zero mean stress correction

Figure 5.8-Figure 5.9 show the data and the predicted results obtained for the as-received SAE1045 and SAE1020 steels at $R \geq 0$. The fatigue properties used to calculate ETS lengths were measured at the respective stress ratios with tensile mean stresses. Unlike the predictions for as-received the SAE1045 steel under zero mean stress (which in general are in good agreement with the corresponding experimental data), those under non-zero mean stress performed conservatively for both finite and infinite life regimes when no correction for mean stress effects was considered (displayed by red lines).

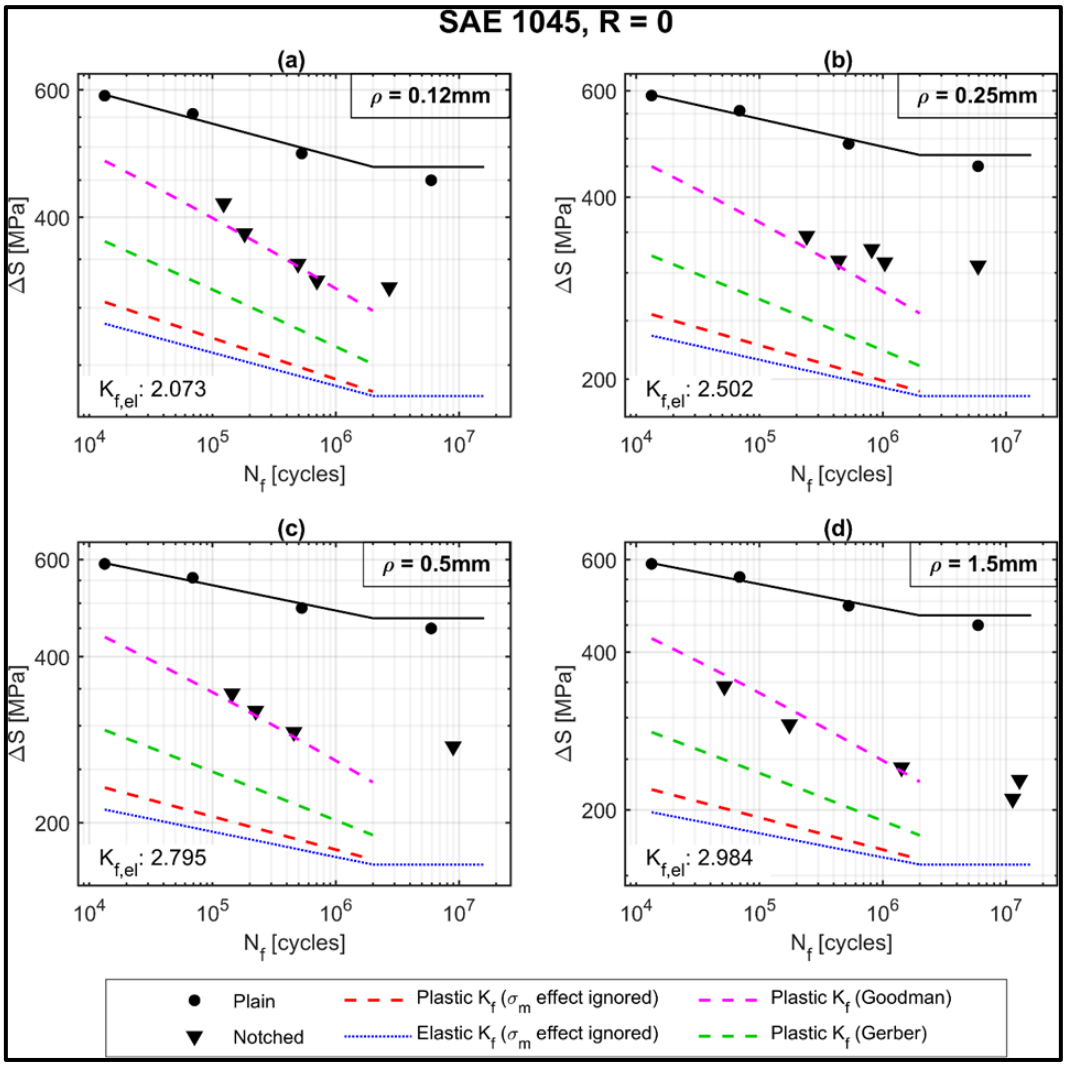

Figure 5.8. S-N curve predictions for notched SAE1045 steel specimens at R=0.

Two classic non-zero mean stress corrections were applied separately: Gerber and Goodman corrections. For SAE1045 at $R = 0$ shown in Figure 5.8, the Goodman approach gives better predictions. However, for SAE1020 at $R = 0.1$ shown in Figure 5.9, the Gerber approach results instead in better predictions. More experimental data on these materials would be needed to verify whether the adherence to Gerber or Goodman is their inherent characteristic.

These comparisons show that significant improvement in the predictions is obtained when the mean stress effect is taken into account properly. Indeed, this effect should not be ignored.

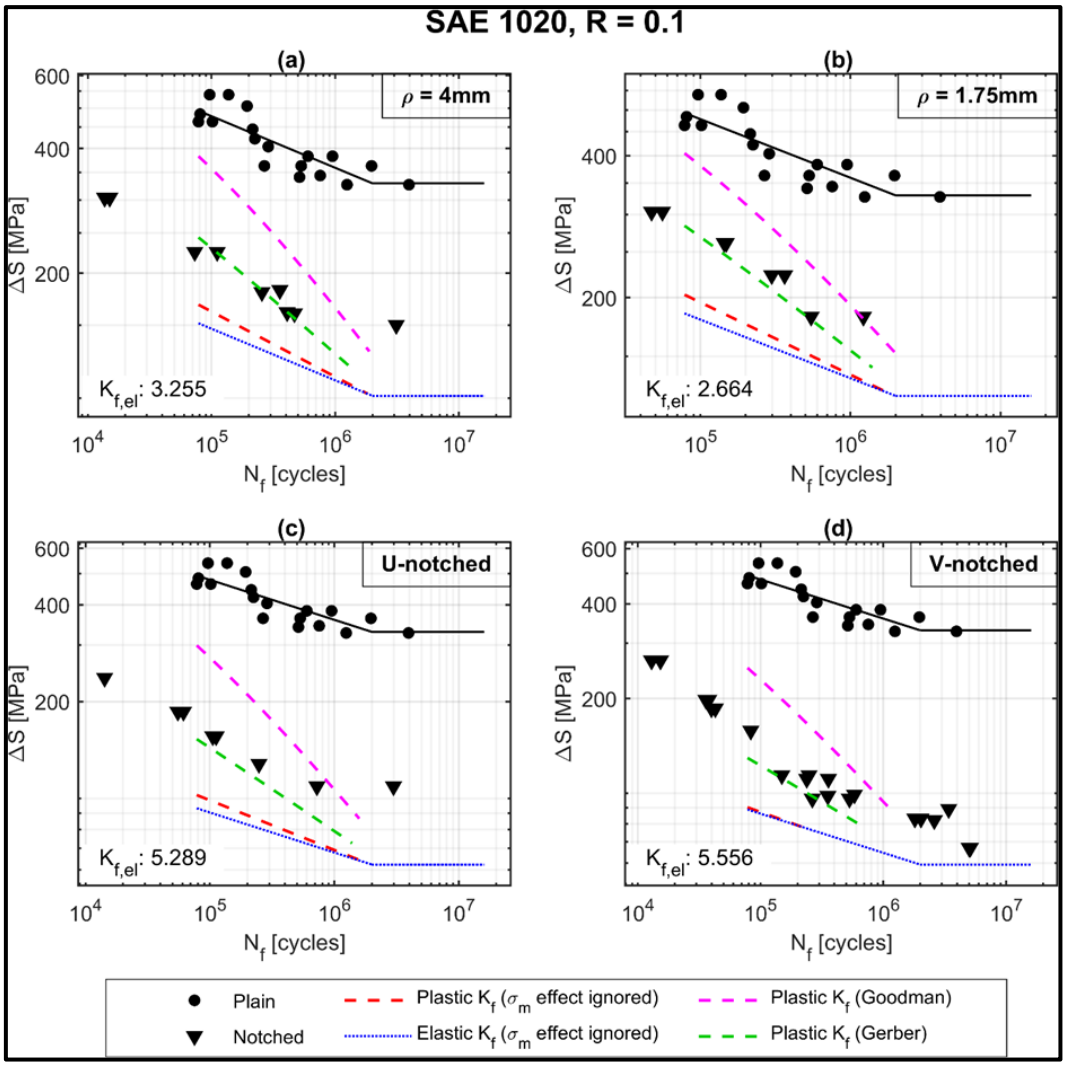

Figure 5.9. S-N curve predictions for notched SAE1020 steel specimens at R=0.1.

6
Conclusion

This work presented an approach to calculate elasto-plastic fatigue stress concentration factors $K_{f,EP}$ based on sound mechanical principles, which can be used to estimate the fatigue strength curves of notched components under small-scale plasticity conditions around their notch tips. The calculations use strain-based Elasto-plastic Fracture Mechanics and short-crack tolerance concepts, which correlate the stress gradients ahead of the notch tips with the short-crack size-dependent fatigue crack growth (FCG) threshold, calculated using the short crack characteristic size a_R at any given R-ratio. The calculation of the elasto-plastic $K_{f,EP}$ uses an iterative process based on Neuber's rule of strain concentration after yielding and on the Ramberg-Osgood cyclic expression to model the strain-hardening behavior of the material.

The predicted $K_{f,EP}$ values have been verified by comparisom with some literature data on SN curves measured on notched specimens. The parameter $K_{f,EP}$ decreases when the nominal stress increases, inducing larger plastic strains. This approach for quantifying the actual notch effects on fatigue strength showed to be more reasonable than simply considering $K_{f,EP}$ equal to 1 at short fatigue lives (10^3 cycles), or $K_{f,EP}$ equal to linear elastic K_f at any stress levels.

For not fully reversed loadings, non-zero mean stress corrections were considered, and a significant improvement in predictions was observed.

6.1
Future works

We plan to conduct experiments to detect non-propagating fatigue cracks departing from notch roots. Firstly, only LE conditions will be applied due to their simplicity compared to the elasto-plastic ones. In addition, we would like to validate the estimative of the maximum non-propagating short crack a_{max} experimentally.

References

[1] R. Ritchie, J. Lankford, "Small fatigue cracks: a statement of the problem and potential solutions", *Materials Science and Engineering*, vol. 84, pp. 11-16. 1986.

[2] C. Shin, R. Smith, "Fatigue crack growth at stress concentrations—the role of notch plasticity and crack closure", *Eng Fract Mech*, vol. 29, pp. 301-315. 1988.

[3] D. Bang, A. Ince, "A short and long crack growth model based on 2-parameter driving force and crack growth thresholds", *Int J Fatigue*, vol. 141, p. 105870. 2020.

[4] M. Hammouda, H. Sallam, H. Osman, "Significance of crack tip plasticity to early notch fatigue crack growth", *Int J Fatigue*, vol. 26, pp. 173-182. 2004.

[5] M. El Haddad, K. Smith, T. Topper, "A strain based intensity factor solution for short fatigue cracks initiating from notches", *Fracture Mechanics, ASTM STP 677*, pp. 274-289. 1979.

[6] W. Illg, "Fatigue tests on notched and unnotched sheet specimens of 2024-T3 and 7075-T6 aluminum alloys and of SAE 4130 steel with special consideration of the life range from 2 to 10,000 cycles", *Journal*, vol., 1956.

[7] C. Kirsch, "Die theorie der elastizitat und die bedurfnisse der festigkeitslehre", *Zeitschrift des Vereines Deutscher Ingenieure*, vol. 42, pp. 797-807. 1898.

[8] C.E. Inglis, "Stresses in a plate due to the presence of cracks and sharp corners", *Trans Inst Naval Archit*, vol. 55, pp. 219-241. 1913.

[9] H. Neuber, Kerbspannungslehre: Theorie der Spannungskonzentration Genaue Berechnung der Festigkeit, Walter de Gruyter GmbH & Co KG2001.

[10] G.N. Savin, Stress distribution around holes, National Aeronautics and Space Administration1970.

[11] W.D. Pilkey, D.F. Pilkey, Z. Bi, Peterson's stress concentration factors, John Wiley & Sons2020.

[12] R. Heywood, Design against fatigue, Chapman and Hall1962.

[13] R.E. Peterson, "Notch sensitivity", *Metal fatigue*, pp. 293-306. 1959.

[14] M.A. Meggiolaro, A.C. de Oliveira Miranda, J.T.P. de Castro, "Short crack threshold estimates to predict notch sensitivity factors in fatigue", *Int J Fatigue*, vol. 29, pp. 2022-2031. 2007.

[15] N.E. Frost, K.J. Marsh, L.P. Pook, Metal fatigue, Courier Corporation1999.

[16] J. Castro, M. Meggiolaro, "Fatigue Design Techniques, vol. 1: High-Cycle Fatigue", *CreateSpace Independent Publishing Platform*. 2016.

[17] H. Abdel-Raouf, T. Topper, A. Plumtree, "A short fatigue crack model based on the nature of the free surface and its microstructure", *Scripta metallurgica et materialia*, vol. 25, pp. 597-602. 1991.

[18] H. Abdel‐Raouf, T. Topper, A. Plumtree, "A model for the fatigue limit and short crack behaviour related to surface strain redistribution",

Fatigue Fract Eng Mater Struct, vol. 15, pp. 895-909. 1992.
[19] M.D. Chapetti, "Fracture mechanics for fatigue design of metallic components and small defect assessment", *Int J Fatigue*, vol. 154, p. 106550. 2022.
[20] K. Sadananda, A. Arcari, A. Vasudevan, "Does a nucleated crack propagate?", *Eng Fract Mech*, vol. 176, pp. 144-160. 2017.
[21] K. Sadananda, S. Sarkar, "Modified Kitagawa diagram and transition from crack nucleation to crack propagation", *Metallurgical and Materials Transactions A*, vol. 44, pp. 1175-1189. 2013.
[22] K. Sadananda, M.N. Babu, A. Vasudevan, "A review of fatigue crack growth resistance in the short crack growth regime", *Materials Science and Engineering: A*, vol. 754, pp. 674-701. 2019.
[23] A. Noroozi, G. Glinka, S. Lambert, "A study of the stress ratio effects on fatigue crack growth using the unified two-parameter fatigue crack growth driving force", *Int J Fatigue*, vol. 29, pp. 1616-1633. 2007.
[24] D. Bang, A. Ince, M. Noban, "Modeling approach for a unified crack growth model in short and long fatigue crack regimes", *Int J Fatigue*, vol. 128, p. 105182. 2019.
[25] D. Bang, A. Ince, L. Tang, "A modification of UniGrow 2-parameter driving force model for short fatigue crack growth", *Fatigue Fract Eng Mater Struct*, vol. 42, pp. 45-60. 2019.
[26] M.A. Antunes, C.R.M. da Silva, E.M.F. do Rêgo, A.C. de Oliveira Miranda, "Stress intensity factor solutions for fretting fatigue using stress gradient factor", *Eng Fract Mech*, vol. 186, pp. 331-346. 2017.
[27] A. Ince, G. Glinka, "Approximation modeling framework for elastic-plastic stress-strain fields near cracks with a small finite crack tip radius", *Theoretical and Applied Fracture Mechanics*, vol. 121, p. 103452. 2022.
[28] N. Dowling, Crack growth during low-cycle fatigue of smooth axial specimens, ASTM International1977.
[29] M. El Haddad, N. Dowling, T. Topper, K. Smith, "J integral applications for short fatigue cracks at notches", *International Journal of Fracture*, vol. 16, pp. 15-30. 1980.
[30] G. Majzoobi, N. Daemi, "The effects of notch geometry on fatigue life using notch sensitivity factor", *Transactions of the Indian Institute of Metals*, vol. 63, pp. 547-552. 2010.
[31] A.H. Committee, Properties and Selection: Irons, Steels, and High-Performance Alloys, ASM International1990.
[32] R.C. Juvinall, K.M. Marshek, Fundamentals of machine component design, 7th ed., John Wiley & Sons2020.
[33] A.C.d.O. Miranda, M.A. Antunes, M.V.G. Alarcón, M.A. Meggiolaro, J.T.P.d. Castro, "Use of the stress gradient factor to estimate fatigue stress concentration factors Kf", *Eng Fract Mech*, vol. 206, pp. 250-266. 2019.
[34] H. Neuber, "Theory of stress concentration for shear-strained prismatical bodies with arbitrary nonlinear stress-strain law". 1961.
[35] M. El Haddad, K. Smith, T. Topper, "Fatigue crack propagation of short cracks", *J Eng Mater Technol*, vol. 101, pp. 42-46. 1979.
[36] M. El Haddad, T. Topper, K. Smith, "Prediction of non propagating cracks", *Eng Fract Mech*, vol. 11, pp. 573-584. 1979.

[37] M. El Haddad, T. Topper, T. Topper, "Fatigue life predictions of smooth and notched specimens based on fracture mechanics". 1981.
[38] J.T.P. Castro, M.A. Meggiolaro, "Fatigue Design Techniques, volume 3: Crack Propagation, Temperature and Statistical Effects", *Journal*, vol., 2016.
[39] M. Yu, D. DuQuesnay, T. Topper, "Notch fatigue behaviour of SAE1045 steel", *Int J Fatigue*, vol. 10, pp. 109-116. 1988.
[40] Z.P. Bažant, "Scaling of quasibrittle fracture: asymptotic analysis", *International Journal of Fracture*, vol. 83, pp. 19-40. 1997.
[41] H. Tada, P.C. Paris, G.R. Irwin, "The stress analysis of cracks", *Handbook, Del Research Corporation*, vol. 34. 1973.
[42] B. Atzori, P. Lazzarin, S. Filippi, "Cracks and notches: analogies and differences of the relevant stress distributions and practical consequences in fatigue limit predictions", *Int J Fatigue*, vol. 23, pp. 355-362. 2001.
[43] B. Atzori, P. Lazzarin, G. Meneghetti, "Fracture mechanics and notch sensitivity", *Fatigue Fract Eng Mater Struct*, vol. 26, pp. 257-267. 2003.
[44] M. Ciavarella, G. Meneghetti, "On fatigue limit in the presence of notches: classical vs. recent unified formulations", *Int J Fatigue*, vol. 26, pp. 289-298. 2004.
[45] B. Atzori, P. Lazzarin, G. Meneghetti, "A unified treatment of the mode I fatigue limit of components containing notches or defects", *International journal of fracture*, vol. 133, pp. 61-87. 2005.
[46] B. Atzori, G. Meneghetti, L. Susmel, "Material fatigue properties for assessing mechanical components weakened by notches and defects", *Fatigue Fract Eng Mater Struct*, vol. 28, pp. 83-97. 2005.
[47] J.T.P. de Castro, M.A. Meggiolaro, A.C. de Oliveira Miranda, H. Wu, A. Imad, N. Benseddiq, "Prediction of fatigue crack initiation lives at elongated notch roots using short crack concepts", *Int J Fatigue*, vol. 42, pp. 172-182. 2012.
[48] E.M.F. do Rêgo, M.A. Antunes, A.C. de Oliveira Miranda, "A methodology for fretting fatigue life estimation using strain-based fracture mechanics", *Eng Fract Mech*, vol. 194, pp. 24-41. 2018.
[49] M. Liu, A.C. de Oliveira Miranda, M.A. Antunes, M.A. Meggiolaro, J.T.P. de Castro, "Plastic stress concentration effects in fatigue strength", *Int J Fatigue*, vol. 168, p. 107394. 2023.
[50] H. Jakubczak, G. Glinka, Calculation of stress intensity factors for cracks subjected to arbitrary non-linear stress fields, European Structural Integrity Society, Elsevier1999, pp. 261-274.
[51] A. Chattopadhyay, G. Glinka, M. El-Zein, J. Qian, R. Formas, "Stress analysis and fatigue of welded structures", *Welding in the World*, vol. 55, pp. 2-21. 2011.
[52] G. Glinka, G. Shen, "Universal features of weight functions for cracks in mode I", *Eng Fract Mech*, vol. 40, pp. 1135-1146. 1991.
[53] D.L. DuQuesnay, T.H. Topper, M. Yu, "The effect of notch radius on the fatigue notch factor and the propagation of short cracks", *Mechanical Engineering Publications, The Behaviour of Short Fatigue Cracks*, pp. 323-335. 1986.
[54] L. Susmel, D. Taylor, "A novel formulation of the theory of critical

distances to estimate lifetime of notched components in the medium-cycle fatigue regime", *Fatigue Fract Eng Mater Struct*, vol. 30, pp. 567-581. 2007.

[55] M. Meggiolaro, J. Castro, "Statistical evaluation of strain-life fatigue crack initiation predictions", *Int J Fatigue*, vol. 26, pp. 463-476. 2004.

[56] Y.L. Wu, S.P. Zhu, J.C. He, D. Liao, Q.Y. Wang, "Assessment of notch fatigue and size effect using stress field intensity approach", *Int J Fatigue*, vol. 149, p. 106279. 2021.

[57] M.A. Meggiolaro, J.T.P. de Castro, "An improved strain-life model based on the Walker equation to describe tensile and compressive mean stress effects", *Int J Fatigue*, vol. 161, p. 106905. 2022.

[58] R.V. Landim, J.T.P.d. Castro, G. Altoé, M.A. Meggiolaro, J.A.C. Velasco, "Notch sensitivity and short cracks tolerance in a super 13Cr stainless steel under sulfide stress corrosion cracking conditions", *Corrosion Reviews*, vol. 41, pp. 57-71. 2023.

Appendix A

This appendix shows a more general formulation than that shown in section 3.3 to calculate a_{max} and K_f for limit between the propagation and non-propagation conditions of cracks. Here, we use a generic value of $f(a/w)$ instead of considering $f(a/w \to 0) \to 1$ for short cracks.

The eq.(3.17) can be written as follows for the tangency:

$$K_{gr}(a_{max}/w) = K_f \cdot \underbrace{\sqrt{\frac{a_R}{a_{max}}} \cdot \left[1 + \left(\frac{a_R}{a_{max}}\right)^{\frac{\gamma}{2}}\right]^{-\frac{1}{\gamma}}}_{h(a_R/a_{max},\ \gamma)} \cdot \frac{1}{f(a_{max}/w)} \tag{0.1}$$

where, the notation $h(a_R/a_{max},\gamma)$ is used to simplify the representation of the equation. Derivating eq.(0.1), we obtain:

$$\frac{\partial}{\partial a}\left[K_{gr}\left(\frac{a_{max}}{w}\right)\right] = K_f \cdot \frac{\partial}{\partial a}\left[\frac{h(a_R/a_{max},\ \gamma)}{f(a_{max}/w)}\right] \tag{0.2}$$

Derivating the eq.(0.2) and then isolating the K_f,

$$\frac{\delta K_{gr}}{\delta a} = K_f \cdot \left(\frac{f \cdot \frac{\delta h}{\delta a} - h \cdot \frac{\delta f}{\delta a}}{f^2}\right)$$

$$\rightarrow \quad K_f = \frac{\delta K_{gr}}{\delta a} \cdot \left(\frac{f^2}{f \cdot \frac{\delta h}{\delta a} - h \cdot \frac{\delta f}{\delta a}}\right) \tag{0.3}$$

where, $f = f(a_{max}/w)$ and $h = h(a_R/a_{max},\gamma)$.

Now, substitute K_f expression into eq.(0.1),

$$K_{gr} - \frac{\delta K_{gr}}{\delta a} \cdot \left(\frac{f \cdot h}{f \cdot \frac{\delta h}{\delta a} - h \cdot \frac{\delta f}{\delta a}}\right) = 0 \tag{0.4}$$

Considering a function $\kappa(a_R/a_{max},\gamma) = 2a_{max}\eta \cdot \left[1 + (a_R/a_{max})^{\gamma/2}\right]$, eq.(0.4) becomes:

$$\frac{\kappa \cdot \partial\left(K_{gr} \cdot f\right)/\partial a + K_{gr} \cdot f}{\kappa \cdot \partial f/\partial a + f} = 0 \qquad (0.5)$$

The eq.(0.5) is more general. And in the case of $f(a_{max}/w) \to 1$, it reproduces the eq.(3.22), which can also be written as below:

$$\kappa \cdot \partial K_{gr}/\delta a + K_{gr} = 0 \qquad (0.6)$$